New insight into the South Tibetan detachment system: Not a single progressive deformation

Dawn A. Kellett[1,2] and Djordje Grujic[1]

Received 7 June 2011; revised 24 January 2012; accepted 31 January 2012; published 21 March 2012.

[1] Low-angle normal faults (LANF), typically regarded as accommodating crustal or lithospheric extension, may also form during lithospheric shortening. The best-studied system of syn-contractional LANFs is the South Tibetan detachment system, a network of low-angle normal sense faults and shear zones that formed coevally with and parallel to south-vergent thrusts during lithospheric shortening accompanying development of the Himalayan orogen. In the eastern Himalaya, there are several across-strike exposures of the South Tibetan detachment system. We present new structural and thermometry data from the eastern Himalaya that demonstrate that the South Tibetan detachment system cannot have formed as a single progressive structure. We characterize and distinguish two distinct structural and tectonic components within the currently recognized system: (1) an extensive diffuse, sheared layer that formed the boundary between strong upper crust and weak, southward-flowing middle crust, and (2) a network of brittle-ductile LANFs that locally exhume, partly excise and overprint the earlier mylonite zone at the topographic break between the Himalayan orogen and the Tibetan plateau. The sheared layer, not a LANF, formed the boundary between upper and middle crust during ductile flow of the middle crust and is extensively exposed in the Himalaya at the base of klippen of upper crustal rocks preserved in Bhutan, along the crest of the Himalaya where it has been excised and exhumed by the brittle-ductile extrusion LANFs, and bounding the cores of the North Himalayan gneiss domes.

Citation: Kellett, D. A., and D. Grujic (2012), New insight into the South Tibetan detachment system: Not a single progressive deformation, *Tectonics*, *31*, TC2007, doi:10.1029/2011TC002957.

1. Introduction

[2] Low-angle normal sense faults (LANFs) are relatively common structures in several orogenic and post-orogenic tectonic environments. They typically juxtapose rocks exhumed from the middle or lower crust in the footwall against upper crustal rocks in the hanging wall, and in many cases, have been found to accommodate lithospheric-scale extension. The formation of normal-sense structures at low angles (≤30°) apparently contradicted conventional fault mechanics [*Anderson*, 1951], which for a time delayed their recognition in the field [e.g., *Armstrong*, 1972; *Davis and Coney*, 1979; *Wernicke and Burchfiel*, 1982]. Although LANFs formed in extensional settings have now been studied intensively for several decades, debate continues about their initial orientations (low-angle or high-angle) [*Axen*, 2007], the relationship between near-surface brittle faulting and ductilely deformed tectonites exhumed in the footwall [*Wernicke*, 2009], the dynamics of coupling and decoupling of mid crust and upper crust [*Wernicke et al.*, 2008] and the amount of extension accommodated (significant or insignificant) at the scale of the lithosphere [e.g., *Wernicke et al.*, 1988; *Anders et al.*, 2006].

[3] More recently, it has become increasingly apparent that orogen strike-parallel LANFs can form during crustal- and lithospheric-scale contraction as well (e.g., in the Himalaya [*Burg et al.*, 1984]; Pamir [*Brunel et al.*, 1994]; Canadian Cordillera [*Carr et al.*, 1987; *Brown and Gibson*, 2006; *Kuiper et al.*, 2006]; U.S. Cordillera [*Wells and Hoisch*, 2008]; Hellenides [*Xypolias and Kokkalas*, 2006; *Ring et al.*, 2007]; Central Alps [*Keller et al.*, 2006]). The tectonic development of LANFs in contractional settings is yet poorly understood. While they have been identified in several orogens, detailed geochronological studies are only now demonstrating their longevity and synchroneity with strike-parallel shortening structures.

[4] The best-studied example of a syn-contractional LANF is the South Tibetan detachment system (STDS), a network of low-angle, top-to-the-north faults and shear zones in the hinterland of the Himalayan orogen [e.g., *Burg and Chen*, 1984; *Burchfiel et al.*, 1992; *Hodges et al.*, 1992; *Brown and Nazarchuk*, 1993; *Makovsky et al.*, 1996; *Carosi et al.*, 1998; *Coleman and Hodges*, 1998; *Wu et al.*, 1998; *Dézes et al.*, 1999; *Edwards et al.*, 1999; *Searle et al.*, 2003; *Cottle et al.*, 2007; *Jessup et al.*, 2008; *Kellett et al.*, 2009; *Leloup et al.*, 2010].

[1]Department of Earth Sciences, Dalhousie University, Halifax, Nova Scotia, Canada.
[2]Now at Geological Survey of Canada, Ottawa, Ontario, Canada.

0278-7407/12/2011TC002957

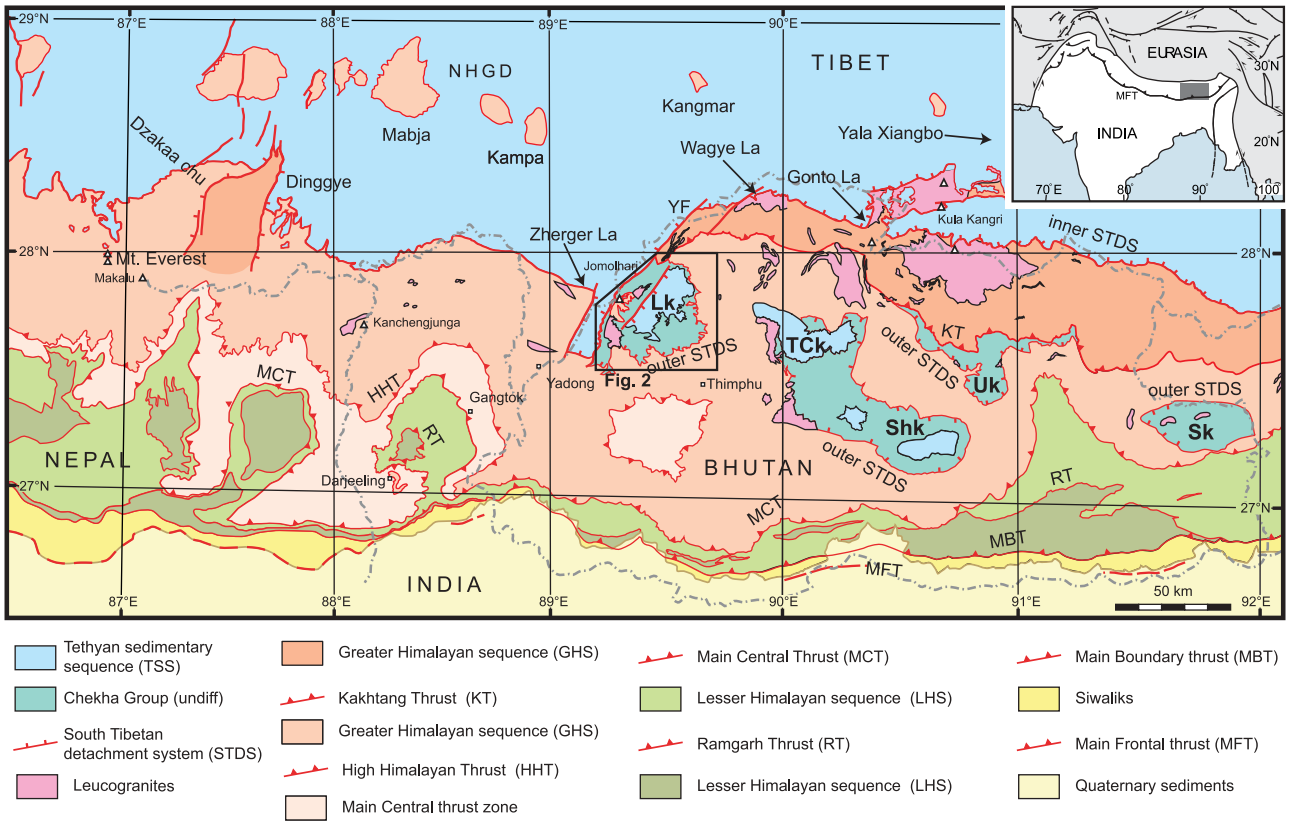

Figure 1. Simplified geological map of Bhutan, Sikkim India and Eastern Nepal with inset showing location of map within the Himalaya-Tibet orogen (modified from *Schelling* [1992], *Goscombe and Hand* [2000], *Goscombe et al.* [2006], *Bhattacharyya and Mitra* [2009], *Kali et al.* [2010], *Kellett et al.* [2009, 2010], and *Leloup et al.* [2010]). O-STDS and I-STDS are outer and inner South Tibetan detachment systems, respectively. HHT, High Himalayan thrust; MBT, Main Boundary thrust; MCT, Main Central thrust; MFT, Main Frontal thrust; KT, Kakhtang thrust; RT, Ramgarh thrust; LF, Lingshi fault; YF, Yadong fault; NHGD, North Himalayan gneiss domes. Klippen from west to east: Lk, Lingshi klippe; TCk, Tang Chu klippe; Shk, Shemgang klippe; Uk, Ura klippe; Sk, Sakteng klippe.

[5] To understand why orogen-parallel syn-collisional LANFs may form in collisional orogens such as the Himalaya, we must establish the relationship between near-surface brittle faults and ductilely deformed tectonites exhumed in the footwall (i.e., are the latter the downdip equivalent of the former, and has there been a change in orientation). Thus far, many studies of the STDS have inferred that all observed top-to-the-north displacement occurred along a single fault zone during a deformation event that progressed to a brittle detachment near the surface [e.g., *Law et al.*, 2004; *Jessup et al.*, 2006; *Cottle et al.*, 2007]. This hypothesis predicts that the multiple structures exposed at the crest of the Himalaya (e.g., the Qomolongma and Lhotse detachments, respectively, in the Everest region [*Searle et al.*, 2003]) are parts of the same shear zone system, in which the lower structure(s) are just deeper parts of the same shear zone and have been exhumed into the footwall of the upper structure(s). Consequently, in the downdip direction (to the north), it follows that these two structures should merge into a single diffuse shear zone due to shear zone widening and deformation being ductile and increasingly pervasive downdip below the brittle-ductile transition. This has been argued for the Dzakaa Chu section north of Everest [e.g., *Cottle et al.*, 2007, Figure 10]. We refer to this hypothesis in this manuscript as a single progressive deformation.

[6] In Bhutan, in the eastern Himalaya, the STDS is exposed along the northern border of the country (Figures 1 and 2) [*Burchfiel et al.*, 1992; *Edwards et al.*, 1996; *Wu et al.*, 1998; *Edwards et al.*, 1999]. However, klippen of upper crustal rocks south of the STDS are soled by top-to-the-north shear zones and are interpreted to be preserved segments of the STDS [*Grujic et al.*, 2002; *Kellett et al.*, 2009; *Chambers et al.*, 2011]. To distinguish these segments from the STDS as it was originally defined, the nomenclature "outer STDS" was introduced in Bhutan [*Kellett et al.*, 2009]. Thus, locally the laterally continuous STDS exposed in the north of Bhutan is referred to as the "inner STDS" and the exposures preserved at the base of the klippen are referred to as the "outer STDS" (Figure 1). Exposures of the outer STDS are south of the crest of the Himalaya. For the STDS to have operated during a single progressive deformation, these segments must be updip continuations of the STDS exposed along the Himalayan

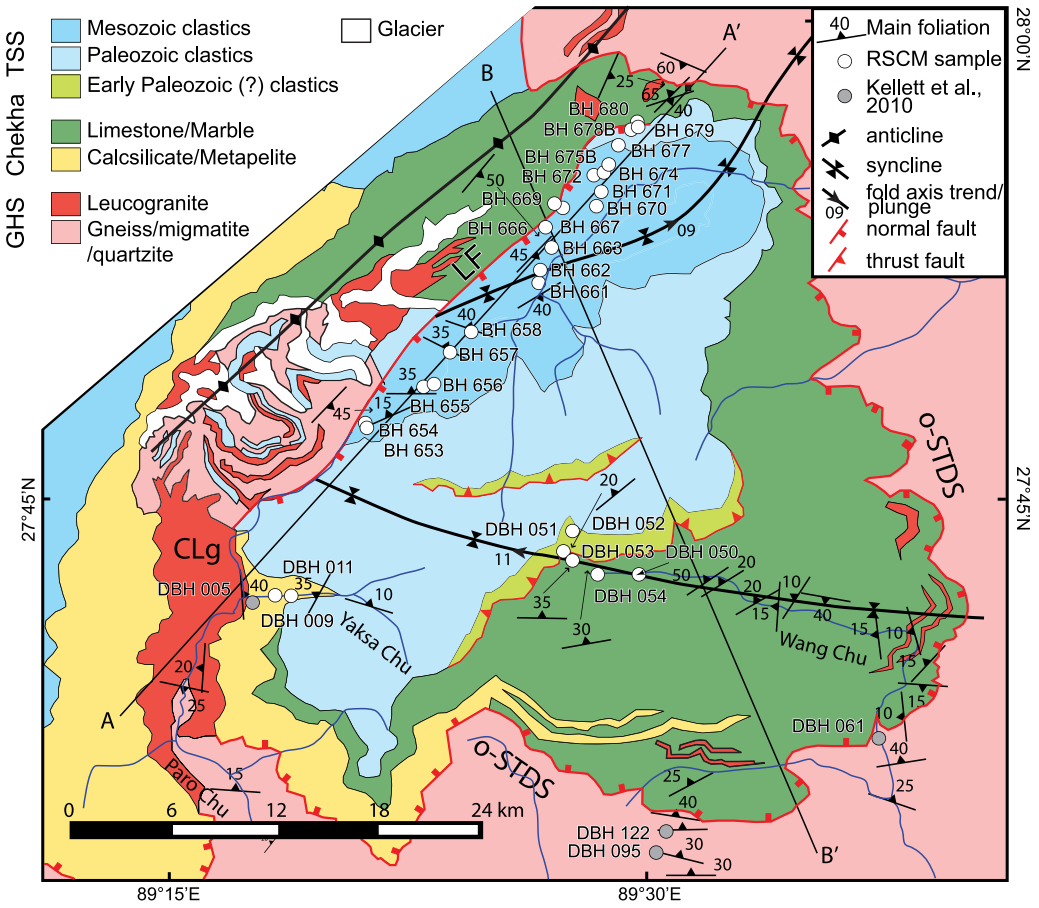

Figure 2. Study area in northwest Bhutan, showing sample locations, structural data and cross-section lines A-A' and B-B' (Figure 3). Map is compiled from *Gansser* [1983], *Kellett et al.* [2009], and our observations. LF, Lingshi fault; CLg, Chung La granite; O-STDS, outer South Tibetan detachment system.

crest. This working hypothesis requires that there is both a ductile lower structure and a discrete upper structure preserved in the outer STDS, with the latter exhuming the former. Thus far the outer STDS has been described as a diffuse ductile shear zone [*Grujic et al.*, 2002; *Kellett et al.*, 2009, 2010], but a putative discrete structure corresponding to an upper structure has yet to be identified. This discrete structure should be identifiable both structurally as a normal fault, and thermometrically (assuming significant post peak-T displacement) by a jump in metamorphic grade from footwall to hanging wall.

[7] Here we test this hypothesis by examining the deformational history and metamorphic field gradient of the Lingshi klippe, the westernmost of the erosional remnants of the STDS in Bhutan. This klippe contains the thickest and most complete section of upper crustal rocks in the Bhutan Himalaya [*Gansser*, 1983], and at its core, the Tethyan sedimentary sequence rocks should be well within the hanging wall of the STDS, such that the entire structural system is preserved. In the sedimentary rocks in the Lingshi klippe there is a lack of metamorphic index minerals commonly used in geothermobarometry (e.g., garnet, biotite, feldspar). Therefore we have used Raman Spectroscopy of Carbonaceous Material (RSCM) thermometry [*Beyssac et al.*, 2002, 2007] to calculate peak metamorphic temperatures for carbonaceous material-bearing lithologies such as black shales from the STDS hanging wall.

2. Geology

2.1. Regional Geology

[8] The Himalayan orogen began to form at ca. 54–50 Ma with the arrival of the Indian plate at the Transhimalayan trench, the southern margin of Asia, following consumption of the intervening Tethys Ocean [*Rowley*, 1996; *de Sigoyer et al.*, 2000; *Leech et al.*, 2005; *Aitchison et al.*, 2007; *Guillot et al.*, 2007]. The several north-dipping first-order structures within the orogen separate sequences of rock of contrasting metamorphic grade, deformation history and/or provenance. South of the Indus-Yarlung suture (separating Indian and Asian crust), the northernmost sequence of rock in the Himalayan orogen is the Tethyan sedimentary sequence (TSS) (Figure 1). The STDS separates un-metamorphosed to low metamorphic-grade Paleozoic to Mesozoic sedimentary rocks of the Tethyan sedimentary sequence from amphibolite- to granulite-facies metamorphic rocks of the Greater Himalayan sequence (GHS) to the south [e.g., *Burchfiel et al.*, 1992]. In places, greenschist to amphibolite-facies metasedimentary rocks are exposed between strands of the STDS. Locally these rocks are termed the Chekha Group

(Bhutan), the Everest Series (eastern Nepal), the Annapurna Yellow Formation (central Nepal) and the Haimantas Group (NW India), and are probably latest Proterozoic to Ordovician in age [*Frank et al.*, 1973; *Gansser*, 1983; *Colchen et al.*, 1986; *Burchfiel et al.*, 1992; *Lombardo et al.*, 1993; *Bhargava*, 1995; *Carosi et al.*, 1999; *Searle et al.*, 2003; *Myrow et al.*, 2009]. Further south, the GHS is separated from greenschist-facies Early Proterozoic to Mesozoic metasedimentary rocks of the Lesser Himalayan sequence (LHS) by the Main Central thrust (MCT). The STDS and the MCT, sub-parallel but opposite-verging structures, were simultaneously active between 22 Ma and at least 18 Ma orogen-wide [i.e., *Godin et al.*, 2006 and references therein], and at least 16 Ma in the Bhutan Himalaya [*Stüwe and Foster*, 2001; *Daniel et al.*, 2003; *Kellett et al.*, 2009; *Chambers et al.*, 2011]. At the base of the LHS is the late Miocene-Pliocene Main Boundary thrust (MBT) [*Meigs et al.*, 1995]. The southernmost lithotectonic unit of the Himalayan orogen is the Sub-Himalaya [*Najman et al.*, 2004], composed of deformed Tertiary foreland basin sediments. The leading edge of deformation is the Main Frontal thrust. At depth, all thrusts appear to root into the Main Himalayan thrust (MHT), the north-dipping basal detachment of the orogen [*Nelson et al.*, 1996].

[9] The STDS is termed a detachment "system" because it consists of one to several normal-sense brittle faults and/or ductile shear zones. In general, the lowest structural levels that record top-to-the-north shear sense movement are high-temperature tectonites of the upper GHS. In the hanging wall of the STDS, the upper deformation front affects weakly metamorphosed TSS rocks. Early top-to-the-south shear sense fabrics have been identified at a few points along the detachment system [e.g., *Yin*, 2006; *Webb et al.*, 2007, and references therein]. To account for some of the complexity of the STD system, the different structures within it have been broadly categorized as "lower" (and generally older) and "upper" (and generally younger), denoting their relative structural positions and ambiguous age relationship (see review by *Godin et al.* [2006]). In fact, the STDS is generally described as being composed of two primary structures: a discrete ductile-brittle detachment and a distributed ductile shear zone in its footwall, both with top-to-the-north kinematics and Miocene displacement [e.g., *Burchfiel et al.*, 1992; *Dézes et al.*, 1999; *Edwards et al.*, 1999; *Godin et al.*, 2006; *Searle et al.*, 2003; *Leloup et al.*, 2010]. In this manuscript, we refer to these two structures as being the upper and lower components of the STDS, respectively. As a reference, at the well-exposed Everest locality, the discrete, brittle-ductile Qomolongma detachment equates to the upper component and the diffuse, ductilely sheared Lhotse detachment equates to the lower component. Note that these are individual structures, while the term STDS refers to the system of structures. Where only a diffuse ductile shear zone is present, such as at Dzakaa Chu [*Cottle et al.*, 2007], we correlate it with the lower component.

[10] The outer STDS in the eastern Himalaya (Figure 1), exposed at the base of klippen of Chekha Group metasedimentary and TSS sedimentary rocks, is distinguished from the continuously exposed segment of the STDS to the north, the inner STDS. The inner and outer STDS have distinct structural, lithological and age characteristics, and are separated by an out-of-sequence thrust, the Kakhtang thrust (Figure 1). In particular, the outer STDS comprises a diffuse ductile shear zone that deforms GHS and Chekha Group rocks [*Grujic et al.*, 2002; *Kellett et al.*, 2009], while the inner STDS comprises an upper ductile-brittle fault (Zherger La detachment of *Wu et al.* [1998], Gonto La detachment of *Edwards et al.* [1996]) with greenschist-facies to unmetamorphosed TSS rocks in the hanging wall and that cuts down into a lower diffuse ductile top-to-the-north shear fabric within amphibolite-granulite grade GHS rocks and leucogranite [*Edwards et al.*, 1996, 1999; *Kellett et al.*, 2009]. Ductile shear on the outer STDS occurred during the Miocene from ca. 22 Ma and had ceased by ca. 12 Ma [*Kellett et al.*, 2009, 2010; *Chambers et al.*, 2011]. Ductile shear on the inner STDS continued after 12 Ma, but ceased by ~11 Ma [*Edwards et al.*, 1996; *Wu et al.*, 1998; *Edwards et al.*, 1999; *Kellett et al.*, 2009].

2.2. Local Geology: Lingshi Klippe

[11] The TSS in the Lingshi klippe, the western-most klippe in Bhutan, comprises early Paleozoic to Cretaceous slate and shale with minor greywacke, conglomerate, sandstone, and limestone (Figures 2, 3, 4a, and 4b) [*Gansser*, 1983]. Sedimentary bedding is locally preserved, and the rocks are variably metamorphosed. Slaty cleavage is generally well developed in the slates and consequently, bedding can be difficult to recognize.

[12] The Chekha Group in the Lingshi klippe varies in both composition and thickness along strike (Figure 3). In the west, the lower Chekha Group comprises garnet-biotite schist with large biotite porphyroblasts (Figure 4g). Locally, abundant tourmaline overgrows the schistosity. The schist is overlain in structural sequence by amphibole-chlorite-biotite-garnet-titanite calc-silicate, chlorite-biotite-muscovite schist and biotite-calcite-bearing quartzite (Figure 4e). In the east, the lower Chekha Group is characterized by biotite-plagioclase-garnet schist, overlain by biotite-muscovite schist (Figure 4h). Tourmaline is present locally. Above the schist are amphibole-chlorite-biotite-titanite calc-silicate, rare calcite-clinopyroxene-titanite calc-silicate, and biotite-muscovite calcarenite (Figure 4f). This unit grades upward into a 1–5 km-thick sequence of muscovite- and quartz-bearing marble (Figure 4d) [*Gansser*, 1983]. The lower Chekha Group in Lingshi klippe is pervasively intruded by leucogranitic sills and dykes.

3. Structural Observations and Interpretations

3.1. Pre-Miocene Deformation

[13] There are several indications for deformation in Chekha Group rocks that predates Miocene ductile shear. At the lowest structural levels, garnets that preserve prograde chemical zoning have both curved and straight internal fabrics at high angle to the external schistosity, and contain inclusions that are finer-grained than the matrix [*Kellett et al.*, 2010]. Stratigraphy is not preserved as the rocks are isoclinally folded at both the outcrop (Figure 5a) and microscopic scales (Figures 4c and 4d), with fold axial planes parallel to the main foliation, resulting in generally monoclinally north- to northwest-dipping strata (Figures 5b and 5c).

[14] Within the TSS, early shortening structures are also evident. Sedimentary bedding (Figure 4b) is folded into

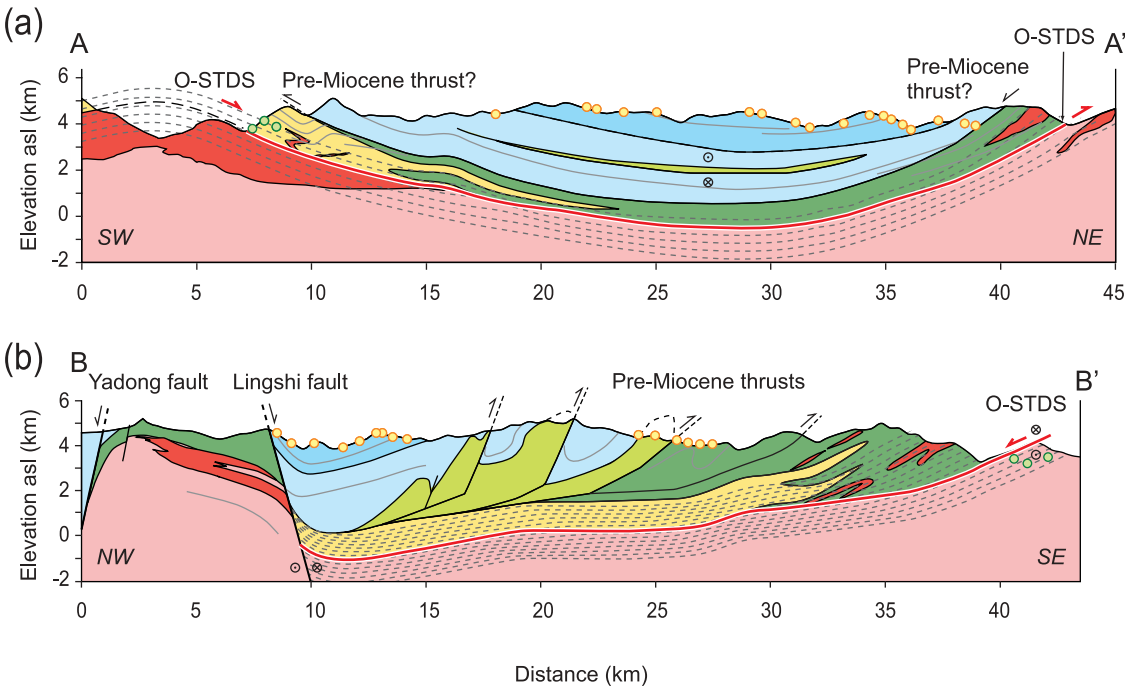

Figure 3. Cross-sections across the Lingshi klippe showing RSCM sample locations. Dashed grey lines indicate extent of O-STDS shear zone deformation. Locations of cross-sections and legend are shown in Figure 2.

upright to reclined folds with wavelengths of 100s of meters (Figure 5d). Several small S- to SE-directed thrusts within the TSS repeat the Paleozoic section (Figures 2 and 3), the largest being the thrust located just north of Shodu along the Wang Chu [*Gansser*, 1983]. Slaty cleavage is well-developed in the slate. Where it is possible to distinguish between slaty cleavage and bedding, the cleavage is everywhere found to be steeper than bedding. We hypothesize that slaty cleavage in the TSS may have been formed during a south-vergent stage of folding and thrusting. However, more detailed structural mapping is needed to unravel the geometry of these early TSS structures.

[15] The contact between the TSS and the Chekha Group along the Yaksa Chu in the west (Figure 2) is characterized by isoclinally folded phyllite of the Chekha Group below (Figure 4c) and fine-grained, quartz- and muscovite-bearing recrystallized limestone with preserved sedimentary bedding above (Figure 4a). Along the Wang Chu in the east, there is a sharp boundary between isoclinally folded Chekha Group marble below (Figure 4d) and TSS lithic sandstone and sandy siltstone above (Figure 4b). The TSS and the Chekha Group are further distinguished by the absence of leucogranitic dykes or sills within the TSS, and their presence in the Chekha Group.

[16] Earliest deformation in the Chekha Group and TSS is compatible with Eohimalayan crustal shortening and thickening, likely following Early Eocene collision of India and Asia, and preceding Neohimalayan activation of the STDS and MCT in the Miocene. We use the terms Eohimalayan and Neohimalayan as described by *Hodges* [2000], in which Eohimalayan deformation is Middle Eocene to Late Oligocene, including collision and subsequent shortening and thickening of Indian crust, and Neohimalayan deformation is Early Miocene to present manifested by peak temperature (T) metamorphism within and exhumation of the GHS between the coeval STDS and MCT. Shortening of the TSS elsewhere in the orogen has been constrained to Eocene-Oligocene [*Ratschbacher et al.*, 1994; *Wiesmayr and Grasemann*, 2002; *Godin*, 2003; *Neumayer et al.*, 2004; *Aikman et al.*, 2008a; *Kellett and Godin*, 2009]. Although in general the sequence youngs upwards from Chekha Group to, and through the TSS rocks, isoclinal folds and transposed bedding in the Chekha Group reveal that the observed "continuous stratigraphy" is only apparent.

3.2. South Tibetan Detachment System

[17] The outer STDS comprises a diffuse ductile shear zone of variable thickness, in which the footwall deformation front is within metapelitic gneiss of the GHS, up to 1 km beneath the contact with the Chekha Group, and is defined by the first appearance of top-to-the-north shear bands (Figure 6) [see also *Kellett et al.*, 2010, Figures 2b and 3]. The high-strain zone penetrates into overlying Chekha Group calc-silicate, mica schist, marble and quartzite which grades upward with decreasing strain into marble and phyllite [*Kellett et al.*, 2010]. The GHS/Chekha contact is therefore a protolith boundary within a 2–3 km-wide ductile shear zone. Miocene leucogranitic dykes and sills are also deformed by ductile shear [*Kellett et al.*, 2009]. Centimeter to mm scale ductile shear bands and associated mineral and stretching lineations indicate top-to-the-north transport. North-vergent shearing of the footwall rocks occurred in the sillimanite stability field during retrograde metamorphism following peak temperature conditions of ~600–800°C with a decreasing preserved peak temperature gradient up-section through the shear zone [*Kellett et al.*, 2010]. Dominant

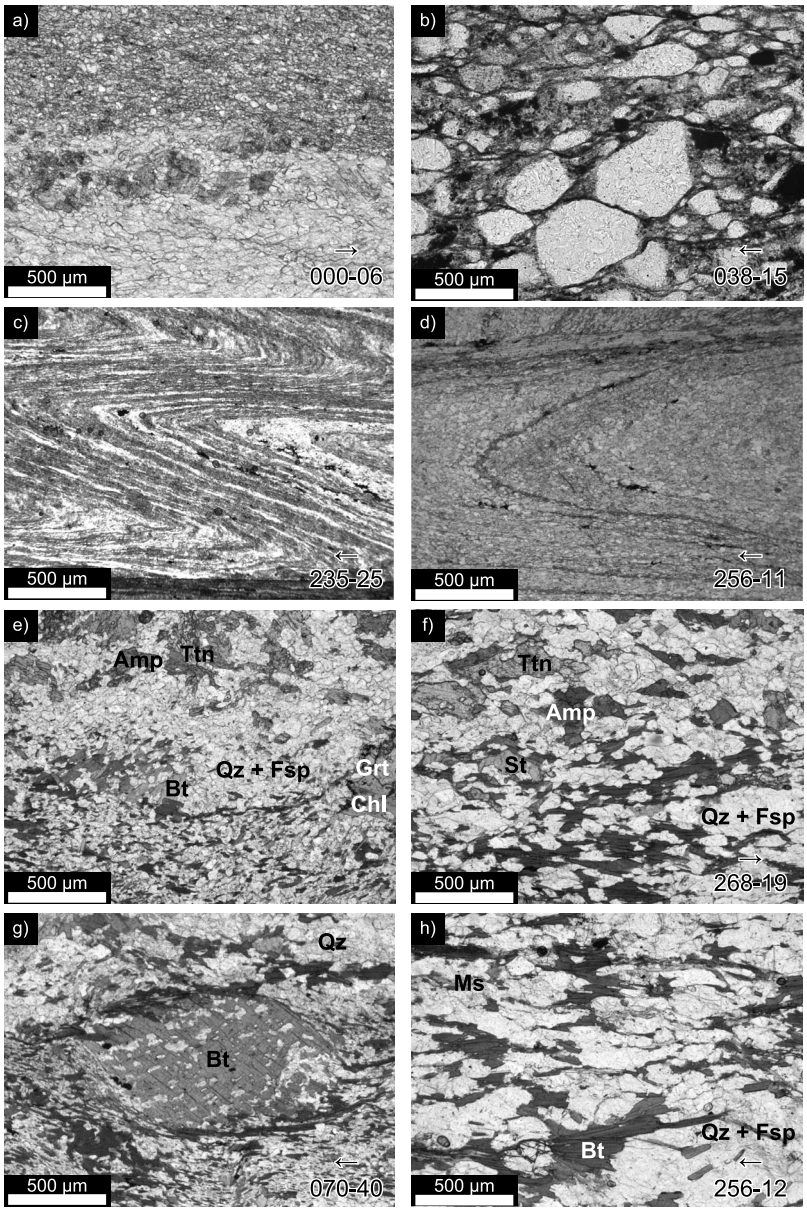

Figure 4. Thin section photomicrographs illustrating lithology and change in metamorphic grade from (a and b) the lowermost TSS, to (c and d) the uppermost Chekha Group, (e and f) the middle Chekha Group (e and f), and (g and h) the lowermost Chekha Group. Figure 4a is TSS limestone and Figure 4b is sandstone, sample DBH 051. Figure 4c is Chekha Group phyllite/slate, sample DBH 011; Figure 4d is impure marble. Figures 4e (DBH 005) and 4f are both biotite- and chlorite-bearing calc-silicate schists. Figure 4g is biotite-chlorite metapelitic schist with biotite porphyroblasts, and Figure 4h is biotite metapelitic schist. Photomicrographs in the left column are collected at the southwest side of the Lingshi klippe along Yaksa Chu, and those in the right column are collected at the southeast and central portions of the Lingshi klippe, along the Wang Chu (Figure 2). Dip and dip direction are recorded for oriented samples, with the arrow pointing in the direction of dip. Mineral abbreviations according to *Whitney and Evans* [2010].

subgrain rotation recrystallization quartz microstructures in syn-deformational leucogranites hosted by Chekha Group rocks indicate deformation temperatures of ~400–500°C [*Kellett et al.*, 2009]. Shearing occurred between ca. 22 - 12 Ma, as determined by U-Pb dating of zircon and monazite, and muscovite $^{40}Ar/^{39}Ar$ cooling ages [*Kellett et al.*, 2009, 2010].

3.3. Low-Amplitude Folding

[18] Several large-scale, upright, low amplitude, non-cylindrical folds with both N-S and E-W axial strike create a broad dome-and-basin geometry for at least 250 km along orogen strike in the GHS at approximately 90° E (Figure 1) [*Gansser*, 1983; *Grujic et al.*, 2002; *Tobgay et al.*, 2010].

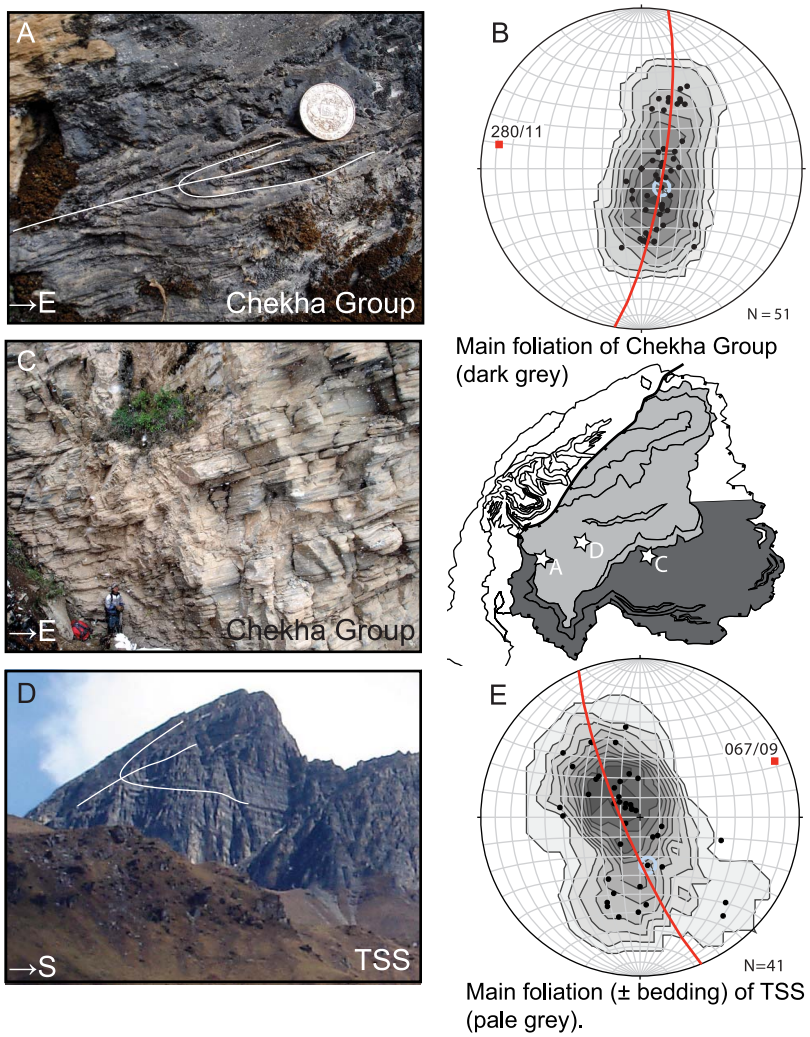

Figure 5. (a–e) Outcrop photographs and stereograms illustrating the main structural styles and cleavage (schistose and slaty for the Chekha Group and TSS, respectively). Chekha Group isoclinal folding and monoclinally dipping beds are shown in Figures 5a and 5c, respectively, while an inclined synform is shown in Figure 5d. Figures 5b and 5e display stereographic projections, lower hemisphere, of poles to cleavage from measurements made within the southern portion of the Chekha Group (shaded with dark grey in inset map below stereogram) and the TSS (shaded with light grey in inset map), respectively. Note that the TSS is dominated by slate, for which cleavage and bedding are difficult to distinguish from one another. Thus, the data presented represents a mixture. Kamb contours, with contour intervals 2σ. Plotted with OSXStereonet (v. 1.7) by N. Cardozo and R. Allmendinger (2011).

Within the Lingshi klippe, there are two first-order synclines at high angle to each other (Figure 2). The axial plane of the southern syncline strikes ~E-W. The fold axis of this syncline plunges 11° toward 280° along the Wang Chu (river) (Figure 5b). The axial surface of the northern syncline strikes NE-SW (Figure 2). In the northeast portion of the TSS, the axis of this syncline plunges 09° toward 067° (Figure 5e). Although our structural data do not constrain a throughgoing N-S striking fold within the Lingshi klippe, the overall map pattern of Bhutan (Figure 1) suggests folding of the MCT + GHS + STDS + TSS package of approximately N-S orientation with a wavelength of ~75 km. The difference in orientation of the fold axis and axial plane may be the result of the scatter of the data, but also may be due to inherited structures in the TSS and dominantly Neohimalayan structures in the Chekha Group.

3.4. Recent Deformation

[19] The oblique-slip Lingshi fault can be traced from northern Bhutan, where it cuts the inner STDS, south through the Lingshi klippe (Figure 2). The fault is sinistral strike-slip with upthrow of the W block [*Gansser*, 1983]. In Sikkim, west of Bhutan, several faults of similar orientation have been observed. The southernmost segment of these, the Gish fault, offsets the MBT [*Mukul et al.*, 2010]. The Lingshi fault may consist of several right-stepping en-échelon segments that strike parallel to the normal faults bounding the Yadong-Gulu graben [*Armijo et al.*, 1986; *Ratschbacher et al.*, 2011]. However, its opposite dip and dip-slip

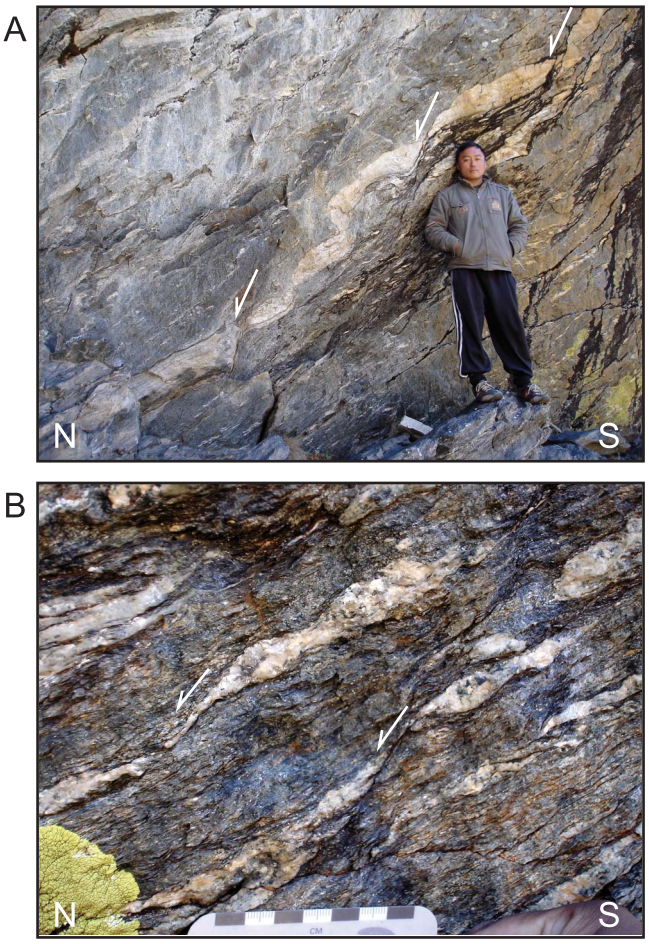

Figure 6. (a) Outcrop photo showing leucogranite hosted by GHS augen gneiss. The leucogranite is pervasively cut by top-down-to-the-north shear bands. (b) Outcrop photo of GHS migmatite gneiss with leucosomes deformed by top-down-to-the-north shear bands. White arrows indicate shear sense.

movement component have resulted in a horst of the Chomolhari range (Figure 2). The Lingshi fault is an active structure, most recently producing an M 5.4 earthquake in 2003 [*Drukpa et al.*, 2006]. The focal solution of this and nearby historic events (e.g., M 6.9 earthquake in Sikkim, 2011) all along strike-slip faults indicate N-S shortening.

4. Raman Spectroscopy of Carbonaceous Material

[20] Raman spectroscopy of carbonaceous material (RSCM) geothermometry is ideal for use in metasedimentary rocks which lack metamorphic indicator minerals, yet commonly contain carbonaceous material [*Beyssac et al.*, 2002, 2004; *Rantitsch et al.*, 2005; *Negro et al.*, 2006]. Carbonaceous material produces several peaks in the first order region (1100–1800 cm^{-1}) of the Raman spectra: three disorder peaks D1, D2 and D3 and the graphite peak G (Figure 7). The RSCM thermometer has been calibrated against the systematic decrease in R2 peak area ratio (D1/G + D1 + D2) in the first order Raman shift between 330 and 650°C [*Beyssac et al.*, 2002; *Rahl et al.*, 2005]. Below 330°C there is no change in R2 ratio; however, it has been observed that the R1 peak height ratio (D1/G) does increase between about 100–350°C, permitting an extension of the thermometer down to 100°C by calibrating against changes in both R1 and R2 ratios [*Rahl et al.*, 2005]. Here we report calculated R1 and R2 ratios, and estimated temperatures using both the calibration of *Beyssac et al.* [2002]:

$$T(^\circ C) = -445\mathbf{R2} + 641 \quad (1)$$

and that of *Rahl et al.* [2005]:

$$T(^\circ C) = 737.3 + 320.9\mathbf{R1} - 1067\mathbf{R2} - 80.638\mathbf{R1}^2 \quad (2)$$

4.1. Sample Description and Preparation

[21] We collected a suite of samples across the Lingshi klippe (Figure 2 and Table 1). Oriented carbonaceous material-bearing samples were collected from both TSS and Chekha Group rocks (sample locations are listed in the auxiliary material).[1] The 24 samples selected are black shale to slate, grey limestone and rare brown sandstone, and contain disseminated fine-grained carbonaceous material. Samples DBH 009 and DBH 011 from the lower Chekha Group are fine-grained mica schist and graphitic phyllite, respectively, and contain discrete graphite crystals.

[22] All samples were cut perpendicular to foliation and parallel to lineation (where present) in order to account for structural heterogeneity [*Beyssac et al.*, 2002]. Highly polished thick (30–100 μm) sections were prepared from these cuts. For those samples with discrete graphite crystals, the crystals were photographed using a reflected light microscope with a 50x objective, and the resulting photomicrographs were used to guide RSCM analyses. Spectra acquisition, raw data and data processing are detailed in the auxiliary material.

4.2. Results

[23] The samples yield a suite of Raman spectra (Figure 7) for which the calculated peak temperatures for TSS and Chekha Group rocks range from ~200 to ~600°C (Table 1 and Figure 8). Since several of the samples were of sufficiently low metamorphic grade that they exhibit no change in R2 ratio (indicative of peak temperature < 330°C) [*Rahl et al.*, 2005], all temperatures reported are calculated using equation (2) (for comparison, temperatures calculated using equation (1) are also reported in Table 1). In general, the TSS rocks exhibit uniformly low peak temperatures ranging from 200 to 350°C. Within the Chekha Group, samples close to the Chekha Group/TSS contact yield ~300°C, with one sample > 400°C. Those close to the GHS/Chekha Group contact yield 300–450°C. For comparison, for Devonian to Triassic age TSS rocks in the hanging wall of the STDS in central Nepal, *Crouzet et al.* [2007] report a similar range of peak metamorphic temperatures of 250–450°C using illite and chlorite crystallinity, vitrinite reflectance, calcite-dolomite and chlorite-chloritoid geothermometers. *Cottle et al.* [2011] report peak metamorphic T in the hanging wall of the STDS in the Dzakaa Chu area of S Tibet of

[1] Auxiliary materials are available in the HTML. doi:10.1029/2011TC002957.

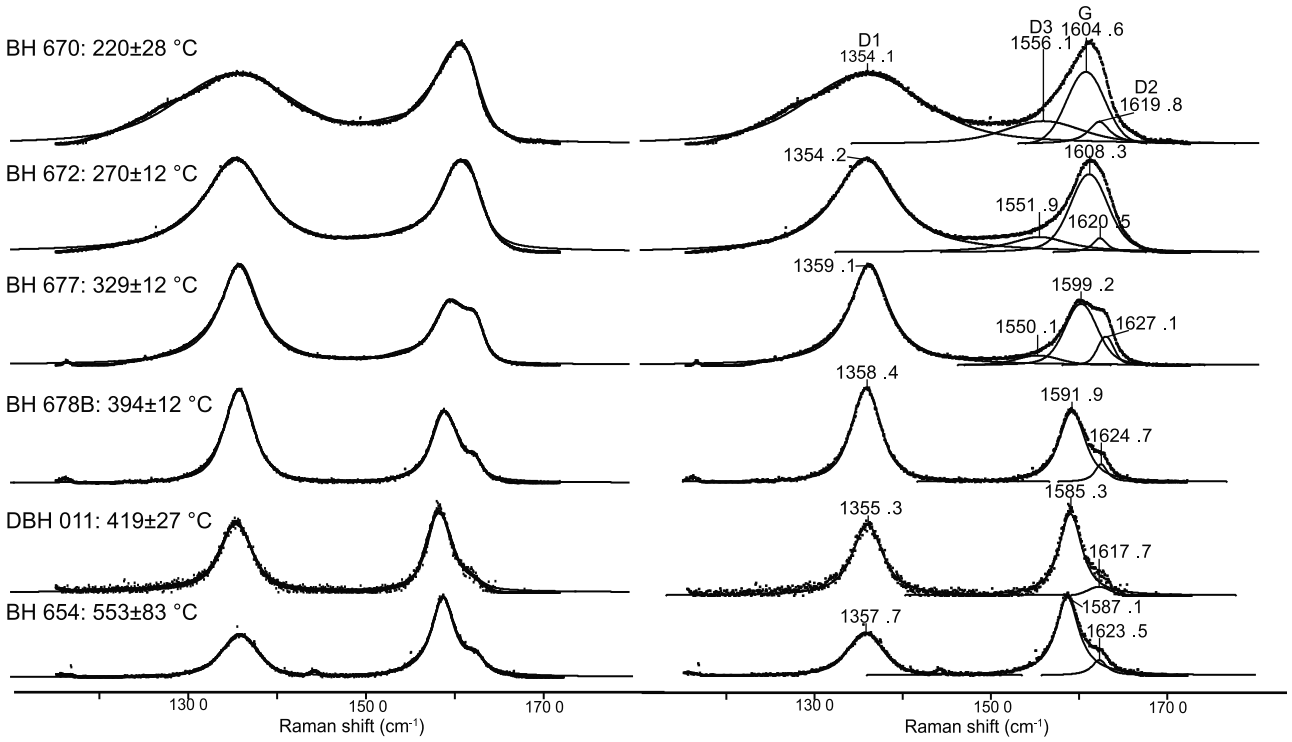

Figure 7. Representative samples illustrating the evolution of observed Raman spectrum and corresponding calculated metamorphic temperatures. Spectra on the right have D1, D2, D3 and G peak positions labeled.

~330–550°C for Chekha Group equivalent and TSS rocks using RSCM and phase equilibria thermometry.

[24] Two TSS samples (BH 653 and BH 654) which yield outlier high RSCM temperatures of 400–600°C (Figure 8) were collected in close proximity to the Lingshi fault. The samples are in the immediate hanging wall, and GHS rocks are exposed in the footwall. We suspect that fluid flow along this fault locally heated these rocks to higher temperature. Samples BH 677, 678B and 680 also yield relatively high RSCM temperatures of ~320–450°C (Figure 8). These samples, collected from the very base of the TSS exposed in the north of the klippe, may overlie a buried leucogranite intrusion.

[25] Our results are compared in Figure 8 against previous PT estimates for GHS and Chekha Group rocks from the Lingshi klippe (DBH 061, DBH 122, DBH 095, DBH 005) and the Ura klippe (CWB-08-04, DBH 068, DBH 071, DBH 063), in which peak temperature conditions were found to predate top-to-the-north shear fabrics, and peak temperatures decrease from a maximum of ~780°C approximately 500 m structurally below the GHS/Chekha Group contact (within the STDS) to ~600°C approximately 250 m structurally above the contact [*Kellett et al.*, 2010]. STDS deformation temperatures in the Chekha Group in the Lingshi klippe were estimated from quartz and feldspar recrystallization microstructure in deformed leucogranites to be ~400–500°C. In the Rongbuk valley north of Mount Everest, quartz *c*-axis fabric opening angles indicate that deformation temperature decreases up section from ~680°C to ~490°C within the top 600 m of the GHS (i.e., still within the STDS) [*Law et al.*, 2011].

5. Discussion

5.1. Structural History of the Bhutan Klippen

[26] The structural evolution of upper-crustal rocks preserved within the Lingshi klippe, including both the Chekha Group and the overlying TSS, can be simplified into three main stages of deformation, summarized in Figure 9. The earliest deformation stage is recorded by schistosity in the Chekha Group, as well as internal fabric in garnet. Garnets preserve an internal fabric that is at high angle in cores and becomes continuous with the external schistosity toward the rims (Figure 9a). Earliest recorded deformation in the TSS is the formation of slaty cleavage (Figure 9a). The axial-planar schistosity preserved in Chekha Group rocks, slaty cleavage and south- and southeast-directed thrusts preserved in TSS rocks may have formed coevally. In that case, differences in style of deformation (recumbent isoclinal folds and bedding transposition in the Chekha Group versus open to tight upright folds and preserved bedding in the TSS) reflect different structural levels (middle crust versus upper crust), and differences in orientation of principal finite strain axes reflect different deformation styles: vertical shortening, horizontal shearing and stretching versus horizontal shortening and crustal thickening, respectively [e.g., *Larson et al.*, 2010]. Such transition in deformation style can occur from hinterland to foreland where the deformation is contemporaneous. Alternatively, this transition can occur

Table 1. Raman Spectroscopy of Carbonaceous Material Results

Sample	Lithology	Tectonic Assemblage	Spectra Acquisition[a]	R1 (Mean)	Error ($\pm1\sigma$)	R2 (Mean)	Error ($\pm1\sigma$)	T[b] (°C) (Mean)	Error (°C) ($\pm1\sigma$)	T[c] (°C) (Mean)	Error (°C) ($\pm1\sigma$)
BH 661	slate	TSS	b	1.21	0.06	0.71	0.02	325	7	248	13
BH 662	slate	TSS	b	0.98	0.04	0.66	0.01	346	3	266	2
BH 658	slate	TSS	b	1.26	0.10	0.74	0.01	311	6	222	20
BH 657	slate	TSS	b	1.36	0.12	0.68	0.01	339	5	300	10
BH 656	slate	TSS	b	1.30	0.04	0.69	0.01	333	3	280	7
BH 663	slate	TSS	b	0.83	0.10	0.66	0.01	347	3	243	12
BH 655	slate	TSS	b	1.19	0.08	0.68	0.02	337	8	274	17
BH 666	slate	TSS	b	1.17	0.22	0.66	0.06	340	22	284	35
BH 667	slate	TSS	b	1.06	0.04	0.70	0.01	330	4	243	14
BH 670	slate	TSS	b	0.83	0.09	0.68	0.03	338	15	220	28
BH 671	slate	TSS	b	0.85	0.10	0.62	0.02	367	11	293	15
BH 672	slate	TSS	b	1.25	0.70	0.70	0.02	331	7	270	12
BH 674	slate	TSS	b	1.30	0.06	0.72	0.01	321	6	251	10
BH 654	slate	TSS	s	0.56	0.22	0.36	0.16	505	49	553	83
BH 653	slate	TSS	b	0.37	0.20	0.34	0.12	488	52	475	82
BH 675B	slate	TSS	b	1.26	0.10	0.73	0.03	315	15	231	43
BH 677	slate	TSS	b	1.68	0.26	0.67	0.01	343	5	329	12
DBH 052	slate	TSS	s	1.65	0.08	0.75	0.02	310	11	252	26
DBH 051	sandstone	TSS	s	1.42	0.07	0.69	0.01	332	4	290	10
BH 678B	slate	TSS	b	1.63	0.17	0.61	0.02	370	10	394	12
BH 680	slate	TSS	b	0.62	0.08	0.44	0.03	444	13	432	17
DBH 053	limestone	Chekha	s	1.82	0.15	0.70	0.01	328	5	302	12
DBH 054	limestone	Chekha	s	1.91	0.12	0.69	0.02	335	10	322	23
DBH 050	limestone	Chekha	s	1.92	0.31	0.69	0.02	336	10	317	20
DBH 009	schist	Chekha	s	0.62	0.23	0.52	0.06	412	29	355	39
DBH 011	phyllite	Chekha	s	0.82	0.08	0.49	0.04	421	17	419	29

[a]For spectra acquisition, 's' denotes that spectra were collected from the polished surface, while 'b' denotes that spectra were collected from beneath transparent grains.
[b]*Beyssac et al.* [2002].
[c]*Rahl et al.* [2005].

between contemporaneous deformation in middle and upper crust (aka orogenic infra- and superstructure [*Culshaw et al.*, 2006]). The above geological evidence suggests that this early stage of orogenic evolution, referred to as the Eohimalayan, was dominated by crustal thickening and related prograde metamorphism.

[27] The second deformation stage involved top-to-the-north shearing in the Miocene (Figure 9b). A broad zone of ductile shear, evidenced by top-to-the-north shear bands and internal boudinage, mineral and stretching lineations and asymmetric folding or boudinage of Miocene leucogranite bodies, has deformed the lower Chekha Group and the top of the GHS (Figure 9b) [*Kellett et al.*, 2009, 2010]. This deformation was coeval with ongoing top-to-the-S shearing at the base of the GHS, along the MCT [*Daniel et al.*, 2003].

[28] The final deformation stage in the Lingshi klippe includes km-scale interference folding of the GHS, Chekha Group and TSS into a dome-and-basin geometry and oblique-slip faulting along the Lingshi and related faults (Figure 9c). Although there are no absolute constraints on the timing of buckling, relative age constraints indicate that it followed cessation of motion on the outer STDS (which is folded by the buckling) at ca. 15.5–12 Ma, and may also have followed cessation of motion on the inner STDS, which is also folded [*Edwards et al.*, 1999] at ca. 10 Ma. Paleomagnetic data from the Lingshi klippe indicate that the folding occurred after ~13 Ma (B. Antolín et al., Disentangling late orogenic deformation stages in the eastern Himalaya (NW Bhutan) by means of pyrrhotite remanences, submitted to *Journal of Structural Geology*, 2011). The Lingshi fault and large transverse structures such as the Yadong-Gulu graben (Figure 1) offset the younger inner STDS. Some of these structures are seismically active now [*Drukpa et al.*, 2006; *Mullick et al.*, 2009; *Ratschbacher et al.*, 2011], making this the most recent deformation that apparently affects the entire Himalayan crust in this region [*Andronicos et al.*, 2007].

[29] These deformation stages reflect the coupling/decoupling history of the upper and middle crust of the Himalaya. Pre-Miocene south-directed shortening structures observed in the TSS and Chekha Group may have been synchronous with Eohimalayan regional prograde metamorphism in the GHS [*Kellett et al.*, 2010], signifying a period of thickening and shortening throughout the upper and middle crust but with different deformation styles. While the STDS was active in the Early and Middle Miocene, the TSS was effectively mechanically decoupled from the GHS, which, for 8–10 million years, underwent south-directed flow, presumably due to significant rheological weakening of the GHS relative to the TSS and LHS, and the pressure gradient caused by greater crustal thickness of the Himalaya-Tibet orogen with respect to the Indian crust in the foreland [i.e., *Beaumont et al.*, 2001]. Once motion on the outer STDS ceased, upper and middle crust were mechanically recoupled, evidenced by km-scale folding of the TSS, GHS and outer STDS. Shearing on the outer STDS ceased at about 15 Ma [*Kellett et al.*, 2009], which provides an upper age constraint for the buckling. Since the inner STDS also appears to be folded in a similar manner [*Edwards et al.*, 1999], the buckling may be younger than 11–10 Ma. This recoupling may have been a result of cooling and hence strengthening of the GHS and consequent loss of rheological layering within this section of the Himalayan crust.

5.2. RSCM and the Thermal Field Gradient Across the Lingshi Klippe

[30] By comparing our RSCM data with phase equilibria peak temperature estimates [*Kellett et al.*, 2010], we constructed the peak temperature field gradient across the entire outer STDS (footwall + high strain zone + hanging wall) of the Lingshi klippe (Figure 8). Though the great variability in thickness of the Chekha Group along strike of the STDS precludes accurate estimation of a unique field gradient representative of the klippe, it can be characterized to a first order. Peak metamorphic temperature decreases steeply but continuously from ~800°C near the top of the GHS to ~300°C in the Chekha Group over a structural thickness of ~1.2 km (Figure 8). Within the Chekha Group high peak metamorphic temperatures coincide with Miocene leucogranitic magmatism and top-to-the-north shear, while low peak temperatures coincide with their absence higher in the section. The peak temperature field gradient across the STDS is an order of magnitude greater than a "normal" continental geothermal gradient (i.e., ~400°C/km, compared to 25–40°C/km).

[31] In summary, the peak temperature profile shown in Figure 8 contains two thermal field gradients. That in the TSS and upper Chekha Group exhibits little to no change in temperature with structural position. Considering our structural observations and Upper Cretaceous illite K-Ar ages in the TSS (Antolín et al., submitted manuscript, XXXX), we interpret the peak temperature field gradient to be Eohimalayan in age, i.e., established prior to the Miocene, during shortening and thickening of the upper crust. Constant peak temperature in a structural package over 4 km thick may occur in a thrust belt by underthrusting (i.e., footwall accretion) dominating overthrusting [e.g., *Bollinger et al.*, 2006; *Célérier et al.*, 2009]. In turn, structural observations and geochronological data (Miocene monazite U-Pb, muscovite $^{40}Ar/^{39}Ar$ and illite K-Ar ages) indicate the steep thermal field gradient at the base of the Chekha Group and top of the GHS to be Neohimalayan, i.e., established in the Miocene. The thermal field gradient is the result of high T metamorphism in the Miocene followed by retrograde shearing along the outer STDS, which telescoped the peak T isotherms under general shear [*Law et al.*, 2011].

[32] Summarizing our data and interpretations, the hypothesis of the South Tibetan detachment system as a deformation progressing to a brittle detachment fails because there is no structural or thermometric evidence for a normal fault akin to the upper component of the STDS in the Lingshi klippe. Moreover, field observations from the Ura klippe [*Kellett et al.*, 2009; 2010], the Shemgang/Black Mountain klippe [*Long and McQuarrie*, 2010; *Corrie et al.*, 2011] and the Radi klippe [*Chambers et al.*, 2011] indicate

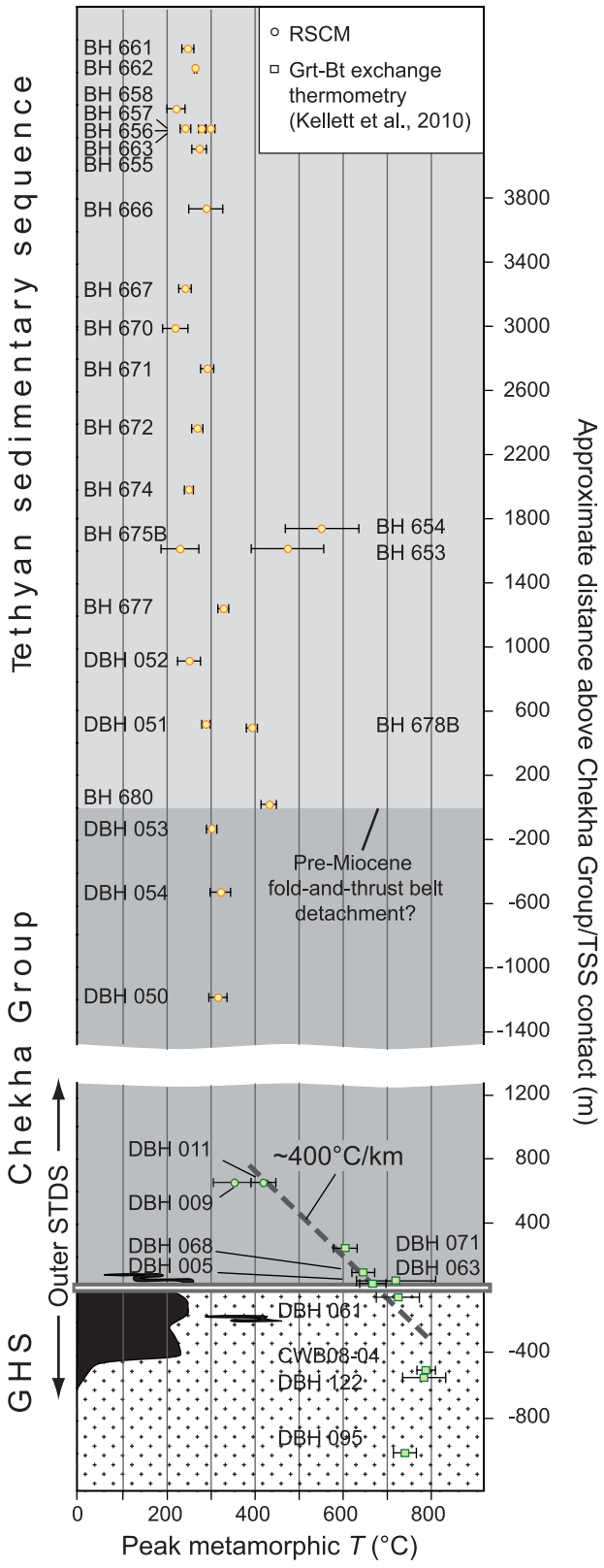

Figure 8. Compilation of peak T in a synthetic vertical structural section. Since thickness of the Chekha Group varies considerably along strike, a nominal structural thickness of 3000 m is displayed, based upon the structural thickness of the Chekha Group, which varies in the Lingshi klippe from ca. 1.5 km to ca. 5 km. Samples DBH 050 and higher are positioned relative to the Chekha Group/TSS contact, while samples below are positioned relative to the GHS/Chekha Group contact. The apparent temperature gradient (dashed grey line) is intended to be a first-order approximation only. RSCM temperatures are calculated using equation (2) [*Rahl et al.*, 2005]. Error bars are $\pm 1\sigma$. Black is leucogranite. Yellow data points are interpreted as an Eohimalayan field gradient and green data points are interpreted as a Neohimalayan field gradient.

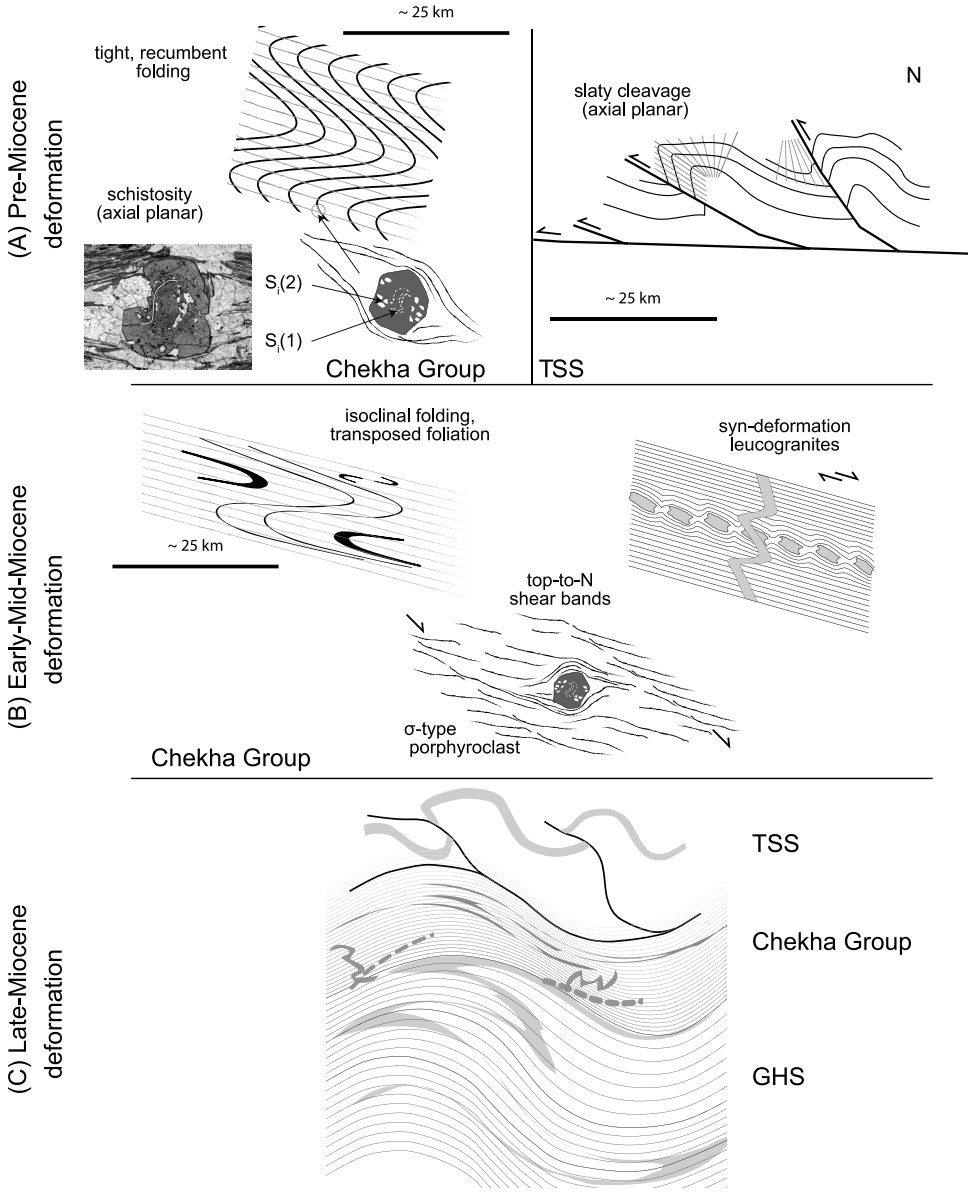

Figure 9. Schematic illustration of structural history of the Chekha Group and TSS in the Lingshi klippe. (a) Eohimalayan, pre-Miocene deformation. (b) Neohimalayan, Early to Mid-Miocene deformation. (c) Neohimalayan, Late Miocene deformation. Field of view in photomicrograph of garnet is 2.5 cm.

that these klippen also lack a discrete detachment, although there is abundant evidence for diffuse top-to-the-north deformation in Chekha Group and upper GHS rocks in all. Instead, the outer STDS is strikingly similar to the STDS as described at Dzakaa Chu [*Cottle et al.*, 2007], a single diffuse ductile shear zone. We re-examine the independent structures of the STDS in terms of their timing, extent and tectonic evolution by comparing them with predictions of thermodynamic modeling.

5.3. Syn-Contraction Hinterland-Directed Deformation

[33] Finite element thermomechanical models of collision of large hot orogens (e.g., the Himalaya) predict three different mechanisms that can produce top-to-the-hinterland shear during contraction. With decreasing amount of relative displacement and increasing dip of the shear plane, these are: (1) channel flow; (2) extrusion of a paleo-channel, and; (3) destabilization of the upper crust above an exhuming dome of channel material [*Beaumont et al.*, 2001, 2004; *Jamieson et al.*, 2004; *Beaumont et al.*, 2006]. Comparison of the structures predicted by the above mechanisms with field data allows us to interpret the origin of the structures within the STDS, and make comparisons between contrasting along and across-strike exposures of the STDS.

5.3.1. Channel Flow

[34] Channel flow of middle or lower crust in a large hot orogen is produced from the combined effects of Couette (shear-driven) and Poiseuille (pressure-driven) flow acting on a weak crustal layer bounded by stronger layers [*Turcotte and Schubert*, 2002]. In channel flow, rocks within the channel experience pervasive shear, with spatiotemporal variations of shear sense controlled by the relative strength

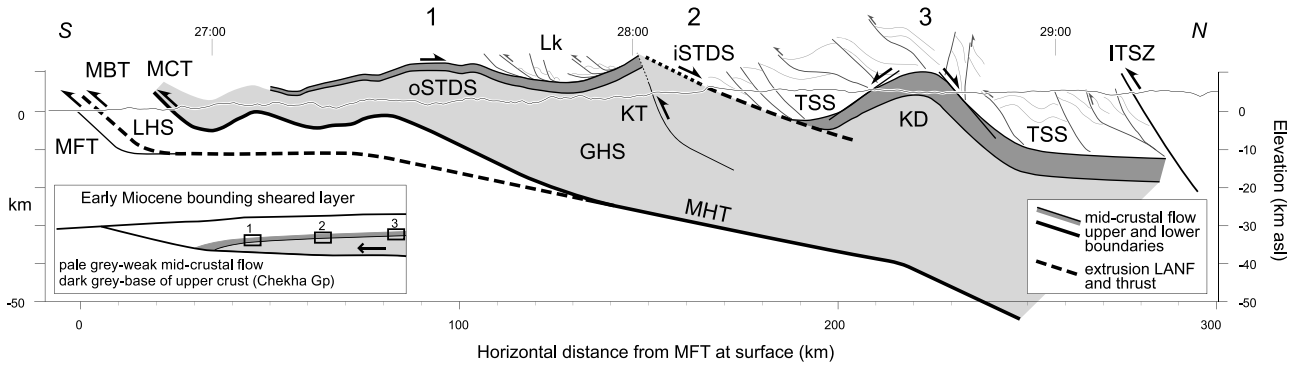

Figure 10. Simplified cross-section through ~89°45′E showing the main structures of the eastern Himalaya. Structures at depth north of 28°N are constrained by INDEPTH data [*Nelson et al.*, 1996]. Fold and thrust belt of the TSS in southern Tibet is modified after a cross-section 30″ west from *Ratschbacher et al.* [1994]. Lk = Linghsi klippe; other abbreviations are described in the text. MHT and MCT, both at surface and at depth, are modified after *Tobgay et al.* [2012]. Solid and dashed lines (shown in legend) indicate interpreted locations of channel flow and extrusion structures in the eastern Himalaya, and dark grey fill shows the location of Chekha Group rocks relative to these structures. Inset shows interpreted development and relative locations in the crust of the now-exhumed mid-crustal sheared layer during early Miocene. Their exhumed equivalents are labeled 1–3 in the main diagram.

of Couette and Poiseuille flow, which in turn are determined by the displacement rates of bounding plates, viscosity of the channel rocks, thickness of the channel, and pressure gradient along the channel [e.g., *Grujic*, 2006]. Where the component of Poiseuille flow prevails, the upper part of the channel should undergo an opposite shear sense compared to the lower part, producing a diffuse bounding sheared layer. The bounding sheared layer locally may or may not preserve a reversal in sense of shear because the relative strength of the two flow components can vary in time and along a channel. Particular distinctions between such a layer and LANFs *sensu stricto* include: (a) the channel-bounding sheared layer does not cut down-section; (b) its base is defined by a reversal in shear sense; (c) it separates upper crust above from previously weak mid-crust below; (d) deformation occurred under ductile conditions and; (e) deformation and metamorphism in the upper crust predates that in the middle crust.

5.3.2. Extrusion LANF

[35] Extrusion in the context of Himalayan-style channel flow has been defined as a process of mid-crustal exhumation acting close to a denudation front beyond the rheological tip of active flow in the mid-crust, in which the mid-crust is exhumed between discrete structures [*Godin et al.*, 2006]. These sub-parallel structures can have opposite sense, resulting in the symmetric extrusion mode [*Beaumont et al.*, 2004] with a LANF at the top, or have the same sense of shear, resulting in the asymmetric thrusting mode [*Beaumont et al.*, 2004], thus no LANF.

[36] As mid-crustal rocks flow toward a low-pressure area, in this case the orogenic front, they are preferentially exhumed with respect to the hinterland and foreland by a combination of focused surface erosion and shearing/faulting on bounding discrete thrust and normal faults [*Beaumont et al.*, 2001]. Normal faults cut down-section, and can excise and expose different sections of the upper to middle crust along and across strike. An extrusion LANF should preserve both brittle and ductile structures, as it exhumes the mid-crust through the brittle-ductile transition toward the surface. Latest motion on an extrusion LANF must post-date ductile flow of the mid-crustal rocks it exhumes.

5.3.3. Destabilization LANF

[37] Doming of a mid-crustal channel and associated destabilization of the upper crust, if it is sufficiently weak, can occur above a ramp or indentor passing beneath the channel [*Jamieson et al.*, 2006]. In addition, Poiseuille flow within a mid-crustal channel produces shear traction on the base of the overburden resulting in a horizontal force [*Gemmer et al.*, 2004] which may further destabilize the upper crust. This force, a function of the ratio of overburden thickness to channel thickness and of the overburden strength, may lead to the failure of the upper crust [*Beaumont et al.*, 2004; *Gemmer et al.*, 2004]. As it is pulled apart, discrete detachment LANFs may form.

5.4. Evaluation of the STDS, Eastern Himalaya

[38] Rather than trying to apply a conventional view of a LANF in an *extensional* setting in which high temperature mylonites are exhumed in the footwall of an ongoing normal fault detachment, progressively rotated into a sub-horizontal position, and overprinted by brittle deformation [e.g., *Mancktelow*, 1990], we find evidence of a more complex sequence of deformation stages for the formation of LANFs in *contractional* settings such as the STDS in the Himalaya. We propose (Figure 10) that the broad, sub-horizontal layer of top-to-the-north ductile shear at the top of the GHS sometimes referred to in the literature as the "lower" component of the STDS and exposed at the base of the Bhutan klippen (outer STDS), at Dzakaa Chu, along the crest of the Himalaya (e.g., Lhotse detachment, Everest; Annapurna detachment, central Nepal) and in the cores of some of the North Himalayan gneiss domes (e.g., Kangmar Dome) [e.g., *Burchfiel et al.*, 1992; *Lee et al.*, 2000; *Grujic et al.*, 2002; *Searle et al.*, 2003; *Cottle et al.*, 2007; *Kellett et al.*, 2010; *Searle*, 2010; *Wagner et al.*, 2010] is an extensive, diffuse,

sheared layer at the boundary between mid- and upper crust that deformed as the result of south-directed mid-crustal flow [*Beaumont et al.*, 2001; *Jamieson et al.*, 2004] during the Early Middle Miocene.

[39] Along the inner STDS in N Bhutan, the sheared layer is cut by a discrete normal fault. There, unlike in the outer STDS of the klippen, Chekha Group rocks are exposed only locally, and we suggest that the kilometers-thick metasedimentary package has been excised by ductile-brittle and brittle normal faulting along an extrusion LANF (Figure 10) during Middle Miocene. This extrusion LANF system appears to be local to the crest of the Himalaya, including the Qomolongma detachment, Everest and the Phu detachment, Annapurna [*Burchfiel et al.*, 1992; *Grujic et al.*, 2002; *Searle et al.*, 2003; *Searle*, 2010; *Kali et al.*, 2010]. In Bhutan, latest motion on this LANF may have been coeval with the out-of-sequence Kakhtang thrust, resulting in extrusion of high-grade GHS rocks [*Warren et al.*, 2011].

[40] North of the eastern Himalaya, high-grade metamorphic rocks are exposed in antiformal gneiss domes (Figure 1) mantled by up to staurolite-kyanite grade Paleozoic metasedimentary rocks, such as the Yala Xiangbo dome to the northeast [e.g., *Aikman et al.*, 2008b], Kangmar dome [e.g., *Lee et al.*, 2000] and Kampa dome [e.g., *Quigley et al.*, 2006] to the northwest, and several others further to the west. Mylonites in the Kangmar dome preserve either top-to-the-north (Kangmar detachment of *Chen et al.* [1990] and *Aoya et al.* [2006]) or both top-to-the-south and top-to-the-north flow shear-sense with a significant component of pure shear [*Lee et al.*, 2000] that overprints an early south-directed shortening fabric. The mylonite fabric has been overprinted by extensional fabrics attributed to doming and exhumation of the gneiss. Doming in the Kangmar Dome may [*Chen et al.*, 1990] or may not [*Lee et al.*, 2000] have generated one or conjugate LANFs. In the Kampa dome, conjugate top-to-the-north and top-to-the-south LANFs on the northern and southern limbs of the dome, respectively, overprint and dip more steeply than the earlier mylonitic top-to-the-north fabric [*Quigley et al.*, 2006]. The ductile shear and overprinting structures described from the Kampa and Kangmar domes are reminiscent of the "lower" and "upper" components of the STD, but the conjugate nature of the overprinting brittle faults is distinct.

[41] Many authors have linked the top-to-the-north ductile flow fabrics exposed in the cores of the domes to the STDS [e.g., *Lee and Whitehouse*, 2007]. Likewise, we interpret this shear zone to be the most internally exposed segment of the laterally pervasive sheared layer formed during mid-crustal flow. The dome bounding structures may be the result of shear traction and destabilization that has tectonically denuded and exposed the bounding sheared layer.

5.5. LANFs and Continental Collision

[42] We have proposed three different ways in which orogen-parallel low-angle normal sense faults/shear zones have formed during continental collision in the Himalayan orogen. While these three tectonic processes have interacted and overprinted one another in the Himalayan orogen, we should not expect to find all three in all collisional orogens.

[43] Sheared layers with an apparent normal-sense displacement that we relate to channel flow require a weak crustal layer that undergoes pressure-driven flow capped by and decoupled from a relatively stronger crustal layer. Thus, for example, a similar sheared layer may exist at present beneath the eastern Tibetan plateau where the lower crust is flowing/tunneling eastward [e.g., *Royden et al.*, 1997, 2008], and depending on erosion conditions may never link to a surface-breaking fault. Numerical thermomechanical modeling results suggest that a channel flow will only form in relatively large and hot orogens such as the Himalaya-Tibet and Grenville orogens [*Beaumont et al.*, 2006], and thus we would not except to find similar sheared layers in relatively small orogens such as the Alps, Pyrenees or Caledonides.

[44] We have argued here that extrusion LANFs in the Himalaya are coupled to channel flow at depth, but they can also form in the absence of crustal flow. Tectonic wedging (in which faults with opposing vergence merge in the updip direction) and wedge extrusion (in which coupled normal and thrust faults merge in the downdip direction) are end-members of extrusion and both can produce similar paired normal and thrust faults [e.g., *Price*, 1986; *Ring and Reischmann*, 2002; *Ring et al.*, 2007], and indeed there is debate among Himalayan researchers that the extrusion LANFs in the western and central Himalaya were alternatively formed only by tectonic wedging [e.g., *Webb et al.*, 2007, 2011]. Extrusion LANFs appear to be likely in both large (Himalaya, Grenville) and smaller (Cordillera, Hellenides, Alps) collisional orogens.

[45] The formation of destabilization LANFs appears to require doming of a weak mid-crust and its dragging a stiffer upper crust, in which case channelized flow may be a requirement for their formation. However, further studies on the structure of this type of dome (e.g., Himalayan gneiss domes) is required to better document the presence/absence and timing of LANFs at their margins.

6. Conclusions

[46] In the Lingshi klippe of Bhutan, Chekha Group and TSS rocks are characterized by pre-Miocene crustal shortening structures. There is a transition in structural style from structurally lower isoclinally folded and transposed Chekha Group rocks to structurally higher upright-folded TSS rocks with preserved bedding. The base of the klippe has been deformed into a broad, ductile top-to-the-north shear zone during the Miocene, the outer STDS. Regional long-wavelength/low amplitude folding of the MCT, GHS, Chekha Group and TSS overprinted all previous structures.

[47] RSCM thermometry data from the Lingshi klippe yield peak metamorphic temperatures of ~200–350°C and apparent constant T with depth for TSS rocks. Chekha Group rocks yield peak temperatures of >300°C, and a steep apparent thermal gradient of ~400°C/km. Neither structural nor thermometric data show evidence for a discrete normal-sense detachment within or between these two units. However, there is a break from Miocene steep peak T field gradient preserved across the STDS. The STDS consistent with expected deformation at the top of a southward-flowing mid-crustal layer, to a near-constant field T in the TSS consistent with crustal thickening dominated by footwall accretion presumably formed during Eohimalayan fold-and-thrust belt development in the TSS.

[48] These structural and thermometric data demonstrate that the syn-contractional STDS could not have formed by

progressive deformation of a single LANF system as hitherto hypothesized. Although the structures of the STDS share the same kinematics, they have formed by at least two processes:

[49] 1. Mid-crustal flow, which produced a diffuse, ductilely sheared layer at the boundary between the mid- and upper crust that does not cut down-section, and that locally preserves a reversal in shear sense. This sheared layer is exposed for >150 km across the strike of the Himalaya, from the STDS klippen to the North Himalayan gneiss domes.

[50] 2. Extrusion, which locally produced ductile-brittle to brittle normal faults that post-date and partly excise the layer of ductile shear produced in 1. This LANF system is exposed only at the crest of the Himalaya.

[51] **Acknowledgments.** We would like to acknowledge assistance and expertise from R. Jamieson, O. Beyssac, I. Coutand, C. Warren, L. Hilchie, and our proficient field crews in Bhutan. RSCM data were collected with the assistance of K. Hewitt in his research laboratory at Dalhousie University. We are grateful to M. Jessup, J. Chambers, N. Rayner, and N. Niemi for insightful reviews which helped to improve the manuscript and to T. Ehlers for editorial handling. This research was partly funded by a Natural Science and Engineering Research Council of Canada (NSERC) Canada Graduate Scholarship-Doctoral and a Killam Memorial PhD scholarship to D. Kellett and a NSERC research grant to D. Grujic.

References

Aikman, A. B., T. M. Harrison, and D. Lin (2008a), Evidence for Early (>44 Ma) Himalayan Crustal Thickening, Tethyan Himalaya, southeastern Tibet, *Earth Planet. Sci. Lett.*, *274*, 14–23, doi:10.1016/j.epsl.2008.06.038.

Aikman, A. B., T. M. Harrison, and D. Lin (2008b), Preliminary results from the Yala-Xiangbo leucogranite dome, SE Tibet, *Himalayan J. Sci.*, *2*, 91.

Aitchison, J. C., J. R. Ali, and A. M. Davis (2007), When and where did India and Asia collide?, *J. Geophys. Res.*, *112*, B05423, doi:10.1029/2006JB004706.

Anders, M. H., N. Christie-Blick, and C. D. Walker (2006), Distinguishing between rooted and rootless detachments: A case study from the Mormon Mountains of southeastern Nevada, *J. Geol.*, *114*(6), 645–664, doi:10.1086/507612.

Anderson, E. M. (1951), *The Dynamics of Faulting*, 2nd ed., 206 pp., Oliver and Boyd, Edinburgh, U. K.

Andronicos, C. L., A. A. Velasco, and J. M. Hurtado Jr. (2007), Large-scale deformation in the India-Asia collision constrained by earthquakes and topography, *Terra Nova*, *19*, 105–119, doi:10.1111/j.1365-3121.2006.00714.x.

Aoya, M., S. Wallis, T. Kawakami, J. Lee, Y. Wang, and H. Maeda (2006), The Malashan gneiss dome in south Tibet: Comparative study with the Kangmar dome with special reference to kinematics of deformation and origin of associated granites, in *Channel Flow, Ductile Extrusion and Exhumation in Continental Collision Zones*, edited by R. D. Law, M. P. Searle, and L. Godin, *Geol. Soc. Spec. Publ.*, *268*, 471–495, doi:10.1144/GSL.SP.2006.268.01.22.

Armijo, R., P. Tapponnier, J. Mercier, and H. Tong-Lin (1986), Quaternary extension in southern Tibet: Field observations and tectonic implications, *J. Geophys. Res.*, *91*, 13,803–13,872, doi:10.1029/JB091iB14p13803.

Armstrong, R. (1972), Low-angle (denudation) faults, hinterland of the Sevier orogenic belt, eastern Nevada and western Utah, *Geol. Soc. Am. Bull.*, *83*(6), 1729–1754, doi:10.1130/0016-7606(1972)83[1729:LDFHOT]2.0.CO;2.

Axen, G. J. (2007), Research focus: Significance of large-displacement, low-angle normal faults, *Geology*, *35*(3), 287, doi:10.1130/0091-7613(2007)35[287:RFSOLL]2.0.CO;2.

Beaumont, C., R. A. Jamieson, M. H. Nguyen, and B. Lee (2001), Himalayan tectonics explained by extrusion of a low-viscosity crustal channel coupled to focused surface denudation, *Nature*, *414*, 738–742, doi:10.1038/414738a.

Beaumont, C., R. A. Jamieson, M. H. Nguyen, and S. Medvedev (2004), Crustal channel flows: 1. Numerical models with applications to the tectonics of the Himalayan-Tibetan orogen, *J. Geophys. Res.*, *109*, B06406, doi:10.1029/2003JB002809.

Beaumont, C., M. H. Nguyen, R. A. Jamieson, and S. Ellis (2006), Crustal flow modes in large hot orogens, in *Channel Flows, Ductile Extrusion and Exhumation in Continental Collision Zones*, edited by R. D. Law, M. P. Searle, and L. Godin, *Geol. Soc. Spec. Publ.*, *268*, 91–145, doi:10.1144/GSL.SP.2006.268.01.05.

Beyssac, O., B. Goffé, C. Chopin, and J. N. Rouzaud (2002), Raman spectra of carbonaceous material in metasediments: A new geothermometer, *J. Metamorph. Geol.*, *20*, 859–871, doi:10.1046/j.1525-1314.2002.00408.x.

Beyssac, O., L. Bollinger, J.-P. Avouac, and B. Goffé (2004), Thermal metamorphism in the lesser Himalaya of Nepal determined from Raman spectroscopy of carbonaceous material, *Earth Planet. Sci. Lett.*, *225*, 233–241, doi:10.1016/j.epsl.2004.05.023.

Beyssac, O., M. Simoes, J.-P. Avouac, K. A. Farley, Y. G. Chen, Y. C. Chan, and B. Goffé (2007), Late Cenozoic metamorphic evolution and exhumation of Taiwan, *Tectonics*, *26*, TC6001, doi:10.1029/2006TC002064.

Bhargava, O. N. (1995), *The Bhutan Himalaya: A Geological Account*, 245 pp., Geol. Surv. of India, Calcutta.

Bhattacharyya, K., and G. Mitra (2009), A new kinematic evolutionary model for the growth of a duplex-an example from the Rangit duplex, Sikkim Himalaya, India, *Gondwana Res.*, *16*, 697–715, doi:10.1016/j.gr.2009.07.006.

Bollinger, L., P. Henry, and J.-P. Avouac (2006), Mountain building in the Nepal Himalaya: Thermal and kinematic model, *Earth Planet. Sci. Lett.*, *244*(1–2), 58–71, doi:10.1016/j.epsl.2006.01.045.

Brown, R. L., and H. D. Gibson (2006), An argument for channel flow in the southern Canadian Cordillera and comparison with Himalayan tectonics, in *Channel Flows, Ductile Extrusion and Exhumation in Continental Collision Zones*, edited by R. D. Law, M. P. Searle, and L. Godin, *Geol. Soc. Spec. Publ.*, *268*, 543–559, doi:10.1144/GSL.SP.2006.268.01.25.

Brown, R. L., and J. H. Nazarchuk (1993), Annapurna detachment fault in the Greater Himalaya of central Nepal, in *Himalayan Tectonics*, edited by P. J. Treloar and M. P. Searle, *Geol. Soc. Spec. Publ.*, *74*, 461–473, doi:10.1144/GSL.SP.1993.074.01.31.

Brunel, M., N. Arnaud, P. Tapponnier, Y. Pan, and Y. Wang (1994), Kongur Shan normal fault: Type example of mountain building assisted by extension (Karakoram fault, eastern Pamir), *Geology*, *22*(8), 707–710, doi:10.1130/0091-7613(1994)022<0707:KSNFTE>2.3.CO;2.

Burchfiel, B. C., Z. Chen, K. V. Hodges, Y. Liu, L. H. Royden, C. Deng, and J. Xu (1992), The South Tibet Detachment System, Himalayan orogen: Extension contemporaneous with and parallel to shortening in a collisional mountain belt, *Spec. Pap. Geol. Soc. Am.*, *269*, 1–41.

Burg, J.-P., and G. M. Chen (1984), Tectonics and structural zonation of southern Tibet, China, *Nature*, *311*, 219–223, doi:10.1038/311219a0.

Burg, J.-P., M. Brunel, D. Gapais, G. M. Chen, and G. H. Liu (1984), Deformation of leucogranites of the crystalline Main Central Sheet in southern Tibet (China), *J. Struct. Geol.*, *6*(5), 535–542, doi:10.1016/0191-8141(84)90063-4.

Carosi, R., B. Lombardo, G. Molli, G. Musumeci, and P. C. Pertusati (1998), The south Tibetan detachment system in the Rongbuk valley, Everest region. Deformation features and geological implications, *J. Southeast Asian Earth Sci.*, *16*(2–3), 299–311, doi:10.1016/S0743-9547(98)00014-2.

Carosi, R., B. Lombardo, G. Musumeci, and P. C. Pertusati (1999), Geology of the higher Himalayan crystallines in Khumbu Himal (eastern Nepal), *J. Asian Earth Sci.*, *17*, 785–803, doi:10.1016/S1367-9120(99)00014-0.

Carr, S. D., R. R. Parrish, and R. L. Brown (1987), Eocene structural development of the Valhalla complex, southeastern British Columbia, *Tectonics*, *6*, 175–196, doi:10.1029/TC006i002p00175.

Célérier, J., T. M. Harrison, O. Beyssac, F. Herman, W. J. Dunlap, and A. A. G. Webb (2009), The Kumaun and Garwhal Lesser Himalaya, India: Part 2. Thermal and deformation histories, *Geol. Soc. Am. Bull.*, *121*(9–10), 1281–1297, doi:10.1130/B26343.1.

Chambers, J., R. Parrish, T. Argles, N. Harris, and M. Horstwood (2011), A short duration pulse of ductile normal shear on the outer South Tibetan detachment in Bhutan: Alternating channel flow and critical taper mechanics of the eastern Himalaya, *Tectonics*, *30*, TC2005, doi:10.1029/2010TC002784.

Chen, Z., Y. Liu, K. Hodges, B. Burchfiel, L. Royden, and C. Deng (1990), The Kangmar dome: A metamorphic core complex in southern Xizang (Tibet), *Science*, *250*, 1552–1556, doi:10.1126/science.250.4987.1552.

Colchen, M., P. Le Fort, and A. Pêcher (1986), *Recherches Géologiques dans l'Himalaya du Népal: Annapurna-Manaslu-Ganesh Himal*, 136 pp., Ed. CNRS, Paris.

Coleman, M., and K. Hodges (1998), Contrasting Oligocene and Miocene thermal histories from the hanging wall and footwall of the South Tibetan detachment in the central Himalaya from $^{40}Ar/^{39}Ar$ thermochronology, Marsyandi Valley, central Nepal, *Tectonics*, *17*(5), 726–740, doi:10.1029/98TC02777.

Corrie, S. L., M. J. Kohn, S. P. Long, N. McQuarrie, and T. Tobgay (2011), P-T data from central Bhutan imply distributed extensional shear at the Black Mountain "klippe", Abstract T21A-2307 presented at 2011 Fall Meeting, AGU, San Francisco, Calif., 5–9 Dec.

Cottle, J. M., M. J. Jessup, D. L. Newell, M. P. Searle, R. D. Law, and M. S. A. Horstwood (2007), Structural insights into the early stages of exhumation along an orogen-scale detachment: The South Tibetan Detachment System, Dzakaa Chu section, Eastern Himalaya, *J. Struct. Geol.*, *29*(11), 1781–1797, doi:10.1016/j.jsg.2007.08.007.

Cottle, J. M., D. J. Waters, D. Riley, O. Beyssac, and M. J. Jessup (2011), Metamorphic history of the South Tibetan Detachment System, Mt. Everest region, revealed by RSCM thermometry and phase equilibria modeling, *J. Metamorph. Geol.*, *29*, 561–582, doi:10.1111/j.1525-1314.2011.00930.x.

Crouzet, C., I. Dunkl, L. Paudel, P. Árkai, T. M. Rainer, K. Balogh, and E. Appel (2007), Temperature and age constraints on the metamorphism of the Tethyan Himalaya in Central Nepal: A multidisciplinary approach, *J. Asian Earth Sci.*, *30*(1), 113–130, doi:10.1016/j.jseaes.2006.07.014.

Culshaw, N., C. Beaumont, and R. A. Jamieson (2006), The orogenic superstructure-infrastructure concept: Revisited, quantified, and revived, *Geology*, *34*, 733–736, doi:10.1130/G22793.1.

Daniel, C. G., L. S. Hollister, R. R. Parrish, and D. Grujic (2003), Exhumation of the Main Central thrust from lower crustal depths, eastern Bhutan Himalaya, *J. Metamorph. Geol.*, *21*, 317–334, doi:10.1046/j.1525-1314.2003.00445.x.

Davis, G. H., and P. J. Coney (1979), Geologic development of the Cordilleran metamorphic core complexes, *Geology*, *7*(3), 120–124, doi:10.1130/0091-7613(1979)7<120:GDOTCM>2.0.CO;2.

de Sigoyer, J., V. Chavagnac, J. Blichert-Toft, I. M. Villa, B. Luais, S. Guillot, M. Cosca, and G. Mascle (2000), Dating the Indian continental subduction and collisional thickening in the northwest Himalaya: Multichronology of the Tso Morari eclogites, *Geology*, *28*, 487–490, doi:10.1130/0091-7613(2000)28<487:DTICSA>2.0.CO;2.

Dézes, P. J., J.-C. Vannay, A. Steck, F. Bussy, and M. Cosca (1999), Synorogenic extension: Quantitative constraints on the age and displacement of the Zanskar shear zone (northwest Himalaya), *Geol. Soc. Am. Bull.*, *111*(3), 364–374, doi:10.1130/0016-7606(1999)111<0364:SEQCOT>2.3.CO;2.

Drukpa, D., A. A. Velasco, and D. I. Doser (2006), Seismicity in the Kingdom of Bhutan (1937–2003): Evidence for crustal transcurrent deformation, *J. Geophys. Res.*, *111*, B06301, doi:10.1029/2004JB003087.

Edwards, M. A., W. S. F. Kidd, J. Li, Y. Yue, and M. Clark (1996), Multistage development of the southern Tibet detachment system near Khula Kangri. New data from Gonto La, *Tectonophysics*, *260*(1–3), 1–19, doi:10.1016/0040-1951(96)00073-X.

Edwards, M. A., A. Pêcher, W. S. F. Kidd, B. C. Burchfiel, and L. H. Royden (1999), Southern Tibet detachment system at Khula Kangri, eastern Himalaya: A large-area, shallow detachment stretching into Bhutan?, *J. Geol.*, *107*, 623–631, doi:10.1086/314366.

Frank, W., G. Hoinkes, C. Miller, F. Purtscheller, W. Richter, and M. Thöni (1973), Relations between metamorphism and orogeny in a typical section of the Indian Himalayas, *Mineral. Petrol.*, *20*, 303–332.

Gansser, A. (1983), *Geology of the Bhutan Himalaya*, 181 pp., Birkhäuser Verlag, Basel, Swizterland.

Gemmer, L., S. J. Ings, S. Medvedev, and C. Beaumont (2004), Salt tectonics driven by differential sediment loading: Stability analysis and finite-element experiments, *Basin Res.*, *16*(2), 199–218, doi:10.1111/j.1365-2117.2004.00229.x.

Godin, L. (2003), Structural evolution of the Tethyan sedimentary sequence in the Annapurna area, central Nepal Himalaya, *J. Asian Earth Sci.*, *22*, 307–328, doi:10.1016/S1367-9120(03)00066-X.

Godin, L., D. Grujic, R. Law, and M. P. Searle (2006), Crustal flow, extrusion, and exhumation in continental collision zones: An introduction, in *Channel Flows, Ductile Extrusion and Exhumation in Continental Collision Zones*, edited by R. D. Law, M. P. Searle, and L. Godin, *Geol. Soc. Spec. Publ.*, *268*, 1–23, doi:10.1144/GSL.SP.2006.268.01.01.

Goscombe, B., and M. Hand (2000), Contrasting P–T paths in the Eastern Himalaya, Nepal: Inverted isograds in a paired metamorphic mountain belt, *J. Petrol.*, *41*, 1673–1719, doi:10.1093/petrology/41.12.1673.

Goscombe, B., D. Grey, and M. Hand (2006), Crustal architecture of the Himalayan metamorphic front in eastern Nepal, *Gondwana Res.*, *10*, 232–255, doi:10.1016/j.gr.2006.05.003.

Grujic, D. (2006), Channel flow and continental collision tectonics: An overview, in *Channel Flows, Ductile Extrusion and Exhumation in Continental Collision Zones*, edited by R. D. Law, M. P. Searle, and L. Godin, *Geol. Soc. Spec. Publ.*, *268*, 25–37, doi:10.1144/GSL.SP.2006.268.01.02.

Grujic, D., L. S. Hollister, and R. R. Parrish (2002), Himalayan metamorphic sequence as an orogenic channel: Insight from Bhutan, *Earth Planet. Sci. Lett.*, *198*, 177–191, doi:10.1016/S0012-821X(02)00482-X.

Guillot, S., A. Replumaz, K. H. Hattori, and P. Strzerzynski (2007), Initial geometry of western Himalaya and ultrahigh-pressure metamorphic evolution, *J. Asian Earth Sci.*, *30*(3–4), 557–564, doi:10.1016/j.jseaes.2007.01.004.

Hodges, K. V. (2000), Tectonics of the Himalaya and southern Tibet from two perspectives, *Geol. Soc. Am. Bull.*, *112*(3), 324–350, doi:10.1130/0016-7606(2000)112<324:TOTHAS>2.0.CO;2.

Hodges, K. V., R. R. Parrish, T. B. Housh, D. R. Lux, B. C. Burchfiel, L. H. Royden, and Z. Chen (1992), Simultaneous Miocene extension and shortening in the Himalayan orogen, *Science*, *258*, 1466–1470, doi:10.1126/science.258.5087.1466.

Jamieson, R. A., C. Beaumont, S. Medvedev, and M. H. Nguyen (2004), Crustal channel flows: 2. Numerical models with implications for metamorphism in the Himalayan-Tibetan orogen, *J. Geophys. Res.*, *109*, B06407, doi:10.1029/2003JB002811.

Jamieson, R. A., C. Beaumont, M. H. Nguyen, and D. Grujic (2006), Provenance of the Greater Himalayan Sequence and associated rocks: Predictions of channel flow models, in *Channel Flows, Ductile Extrusion and Exhumation in Continental Collision Zones*, edited by R. D. Law, M. P. Searle, and L. Godin, *Geol. Soc. Spec. Publ.*, *268*, 165–182, doi:10.1144/GSL.SP.2006.268.01.07.

Jessup, M. J., R. D. Law, M. P. Searle, and M. S. Hubbard (2006), Structural evolution and vorticity of flow during extrusion and exhumation of the Greater Himalayan Slab, Mount Everest Massif, Tibet/Nepal: Implications for orogen-scale flow partitioning, in *Channel Flows, Ductile Extrusion and Exhumation in Continental Collision Zones*, edited by R. D. Law, M. P. Searle, and L. Godin, *Geol. Soc. Spec. Publ.*, *268*, 379–413, doi:10.1144/GSL.SP.2006.268.01.18.

Jessup, M. J., J. M. Cottle, M. P. Searle, R. D. Law, D. L. Newell, R. J. Tracy, and D. J. Waters (2008), PTtD paths of Everest Series schist, Nepal, *J. Metamorph. Geol.*, *26*(7), 717–739, doi:10.1111/j.1525-1314.2008.00784.x.

Kali, E., P. H. Leloup, N. Arnaud, G. Mahéo, D. Liu, E. Boutonnet, J. Van der Woerd, X. Liu, J. Liu-Zeng, and H. Li (2010), Exhumation history of the deepest central Himalayan rocks, Ama Drime range: Key pressure-temperature-deformation-time constraints on orogenic models, *Tectonics*, *29*, TC2014, doi:10.1029/2009TC002551.

Keller, L. M., B. Fügenschuh, M. Hess, B. Schneider, and S. M. Schmid (2006), Simplon fault zone in the western and central Alps: Mechanism of Neogene faulting and folding revisited, *Geology*, *34*, 317–320, doi:10.1130/G22256.1.

Kellett, D. A., and L. Godin (2009), Pre-Miocene deformation of the Himalayan superstructure, Hidden valley, central Nepal, *J. Geol. Soc.*, *166*, 261–275, doi:10.1144/0016-76492008-097.

Kellett, D. A., D. Grujic, and S. Erdmann (2009), Miocene structural reorganization of the South Tibetan detachment, eastern Himalaya: Implications for continental collision, *Lithosphere*, *1*, 259–281, doi:10.1130/L56.1.

Kellett, D. A., D. Grujic, C. Warren, J. M. Cottle, R. A. Jamieson, and T. Tenzin (2010), Metamorphic history of a syn-convergent orogen parallel detachment: The South Tibetan detachment system, Bhutan Himalaya, *J. Metamorph. Geol.*, *28*, 785–808, doi:10.1111/j.1525-1314.2010.00893.x.

Kuiper, Y. D., P. F. Williams, and S. Kruse (2006), Possibility of channel flow in the southern Canadian Cordillera: A new approach to explain existing data, in *Channel Flows, Ductile Extrusion and Exhumation in Continental Collision Zones*, edited by R. D. Law, M. P. Searle, and L. Godin, *Geol. Soc. Spec. Publ.*, *268*, 589–611, doi:10.1144/GSL.SP.2006.268.01.27.

Larson, K. P., L. Godin, and R. A. Price (2010), Relationships between displacement and distortion in orogens: Linking the Himalayan foreland and hinterland in central Nepal, *Geol. Soc. Am. Bull.*, *122*, 1116–1134, doi:10.1130/B30073.1.

Law, R. D., M. P. Searle, and R. L. Simpson (2004), Strain, deformation temperatures and vorticity of flow at the top of the Greater Himalayan Slab, Everest Massif, Tibet, *J. Geol. Soc.*, *161*, 305–320, doi:10.1144/0016-764903-047.

Law, R., M. J. Jessup, M. Searle, M. Francis, D. Waters, and J. M. Cottle (2011), Telescoping of isotherms beneath the South Tibetan Detachment System, Mount Everest Massif, *J. Struct. Geol.*, *33*, 1569–1594, doi:10.1016/j.jsg.2011.09.004.

Lee, J., and M. J. Whitehouse (2007), Onset of mid-crustal extensional flow in southern Tibet: Evidence from U/Pb zircon ages, *Geology*, *35*, 45–48, doi:10.1130/G22842A.1.

Lee, J., B. R. Hacker, W. S. Dinklage, Y. Wang, P. Gans, A. Calvert, J. Wan, W. Chen, A. E. Blythe, and W. McClelland (2000), Evolution of the Kangmar Dome, southern Tibet: Structural, petrologic, and

thermochronologic constraints, *Tectonics*, *19*, 872–895, doi:10.1029/1999TC001147.

Leech, M. L., S. Singh, A. K. Jain, S. L. Klemperer, and R. M. Manickavasagam (2005), The onset of India–Asia continental collision: Early, steep subduction required by the timing of UHP metamorphism in the western Himalaya, *Earth Planet. Sci. Lett.*, *234*, 83–97, doi:10.1016/j.epsl.2005.02.038.

Leloup, P. H., G. Mahéo, N. Arnaud, E. Kali, E. Boutonnet, D. Liu, X. Liu, and H. Li (2010), The South Tibet detachment shear zone in the Dinggye area: Time constraints on extrusion models of the Himalayas, *Earth Planet. Sci. Lett.*, *292*, 1–16, doi:10.1016/j.epsl.2009.12.035.

Lombardo, B., P. Pertusati, and S. Borghi (1993), Geology and tectonomagmatic evolution of the eastern Himalaya along the Chomolungma-Makalu transect, in *Himalayan Tectonics*, edited by P. J. Treloar and M. P. Searle, *Geol. Soc. Spec. Publ.*, *74*, pp. 341–355, doi:10.1144/GSL.SP.1993.074.01.23.

Long, S., and N. McQuarrie (2010), Placing limits on channel flow: Insights from the Bhutan Himalaya, *Earth Planet. Sci. Lett.*, *290*, 375–390, doi:10.1016/j.epsl.2009.12.033.

Makovsky, Y., S. L. Klemperer, H. Liyan, and L. Deyuan (1996), Structural elements of the southern Tethyan Himalaya crust from wide-angle seismic data, *Tectonics*, *15*, 997–1005, doi:10.1029/96TC00310.

Mancktelow, N. S. (1990), The Simplon fault zone, *Beitr. Geol. Karte Schweiz*, *163*, 5–74.

Meigs, A. J., D. W. Burbank, and R. A. Beck (1995), Middle-late Miocene (>10 Ma) formation of the Main Boundary thrust in the western Himalaya, *Geology*, *23*, 423–426, doi:10.1130/0091-7613(1995)023<0423:MLMMFO>2.3.CO;2.

Mukul, M., S. Jade, A. K. Bhattacharyya, and K. Bhusan (2010), Crustal shortening in convergent orogens: Insights from global positioning system (GPS) measurements in northeast India, *J. Geol. Soc. India*, *75*, 302–312, doi:10.1007/s12594-010-0017-9.

Mullick, M., F. Riguzzi, and D. Mukhopadhyay (2009), Estimates of motion and strain rates across active faults in the frontal part of eastern Himalayas in North Bengal from GPS measurements, *Terra Nova*, *21*, 410–415, doi:10.1111/j.1365-3121.2009.00898.x.

Myrow, P. M., N. C. Hughes, M. P. Searle, C. M. Fanning, S. C. Peng, and S. K. Parcha (2009), Stratigraphic correlation of CambrianOrdovician deposits along the Himalaya: Implications for the age and nature of rocks in the Mount Everest region, *Geol. Soc. Am. Bull.*, *121*, 323–332, doi:10.1130/B26384.1.

Najman, Y., K. Johnson, N. White, and G. Oliver (2004), Evolution of the Himalayan foreland basin, NW India, *Basin Res.*, *16*, 1–24, doi:10.1111/j.1365-2117.2004.00223.x.

Negro, F., O. Beyssac, B. Goffé, O. Saddiqi, and M. L. Bouybaouène (2006), Thermal structure of the Alboran Domain in the Rif (northern Morocco) and the Western Betics (southern Spain). Constraints from Raman spectroscopy of carbonaceous material, *J. Metamorph. Geol.*, *24*, 309–327, doi:10.1111/j.1525-1314.2006.00639.x.

Nelson, K. D., et al. (1996), Partially molten middle crust beneath southern Tibet: Synthesis of Project INDEPTH results, *Science*, *274*, 1684–1688, doi:10.1126/science.274.5293.1684.

Neumayer, J., G. Wiesmayr, C. Janda, B. Grasemann, and E. Draganits (2004), Eohimalayan fold and thrust belt in the NW-Himalaya (Lingti-Pin Valleys): Shortening and depth to detachment calculation, *Aust. J. Earth Sci.*, *95*, 28–36.

Price, R. A. (1986), The southeastern Canadian Cordillera: Thrust faulting, tectonic wedging, and delamination of the lithosphere, *J. Struct. Geol.*, *8*, 239–254, doi:10.1016/0191-8141(86)90046-5.

Quigley, M., Y. Liangjun, L. Xiaohan, C. J. L. Wilson, M. Sandiford, and D. Phillips (2006), $^{40}Ar/^{39}Ar$ thermochronology of the Kampa Dome, southern Tibet: Implications for tectonic evolution of the North Himalayan gneiss domes, *Tectonophysics*, *421*, 269–297, doi:10.1016/j.tecto.2006.05.002.

Rahl, J. M., K. M. Anderson, M. T. Brandon, and C. Fassoulas (2005), Raman spectroscopic carbonaceous material thermometry of low-grade metamorphic rocks: Calibration and application of tectonic exhumation in Crete, Greece, *Earth Planet. Sci. Lett.*, *240*, 339–354, doi:10.1016/j.epsl.2005.09.055.

Rantitsch, G., R. F. Sachsenhofer, C. Hasenhüttl, B. Russegger, and T. Rainer (2005), Thermal evolution of an extensional detachment as constrained by organic metamorphic data and thermal modeling: Graz Paleozoic Nappe Complex (Eastern Alps), *Tectonophysics*, *411*, 57–72, doi:10.1016/j.tecto.2005.08.022.

Ratschbacher, L., W. Frisch, G. Liu, and C. Chen (1994), Distributed deformation in southern and western Tibet during and after the India-Asia collision, *J. Geophys. Res.*, *99*, 19,917–19,945, doi:10.1029/94JB00932.

Ratschbacher, L., I. Krumrei, M. Blumenwitz, M. Staiger, R. Gloaguen, B. V. Miller, S. D. Samson, M. A. Edwards, and E. Appel (2011), Rifting and strike-slip shear in central Tibet and the geometry, age and kinematics of upper crustal extension in Tibet, *Geol. Soc. Lond. Spec. Publ.*, *353*, 127–163, doi:10.1144/SP353.8.

Ring, U., and T. Reischmann (2002), The weak and superfast Cretan detachment, Greece: Exhumation at subduction rates in extruding wedges, *J. Geol. Soc.*, *159*, 225, doi:10.1144/0016-764901-150.

Ring, U., J. Glodny, T. Will, and S. Thomson (2007), An Oligocene extrusion wedge of blueschist-facies nappes on Evia, Aegean Sea, Greece: Implications for the early exhumation of high-pressure rocks, *J. Geol. Soc.*, *164*, 637–652, doi:10.1144/0016-76492006-041.

Rowley, D. B. (1996), Age of initiation of collision between India and Asia: A review of stratigraphic data, *Earth Planet. Sci. Lett.*, *145*, 1–13, doi:10.1016/S0012-821X(96)00201-4.

Royden, L. H., B. C. Burchfiel, R. W. King, E. Wang, Z. Chen, F. Shen, and Y. Liu (1997), Surface deformation and lower crustal flow in eastern Tibet, *Science*, *276*, 788, doi:10.1126/science.276.5313.788.

Royden, L. H., B. C. Burchfiel, and R. D. van der Hilst (2008), The geological evolution of the Tibetan Plateau, *Science*, *321*, 1054–1058, doi:10.1126/science.1155371.

Schelling, D. (1992), The tectonostratigraphy and structure of the eastern Nepal Himalaya, *Tectonics*, *11*, 925–943, doi:10.1029/92TC00213.

Searle, M. P. (2010), Low-angle normal faults in the compressional Himalayan orogen; Evidence from the Annapurna-Dhaulagiri Himalaya, Nepal, *Geosphere*, *6*, 296–315, doi:10.1130/GES00549.1.

Searle, M., R. L. Simpson, R. D. Law, R. R. Parrish, and D. J. Waters (2003), The structural geometry, metamorphic and magmatic evolution of the Everest massif, High Himalaya of Nepal-South Tibet, *J. Geol. Soc.*, *160*, 345–366, doi:10.1144/0016-764902-126.

Stüwe, K., and D. Foster (2001), $^{40}Ar/^{39}Ar$, pressure, temperature and fission track constraints on the age and nature of metamorphism around the main central thrust in the eastern Bhutan Himalaya, *J. Asian Earth Sci.*, *19*, 85–95, doi:10.1016/S1367-9120(00)00018-3.

Tobgay, T., S. Long, N. McQuarrie, M. N. Ducea, and G. Gehrels (2010), Using isotopic and chronologic data to fingerprint strata: Challenges and benefits of variable sources to tectonic interpretations, the Paro Formation, Bhutan Himalaya, *Tectonics*, *29*, TC6023, doi:10.1029/2009TC002637.

Tobgay, T., N. McQuarrie, S. P. Long, M. J. Kohn, and S. L. Corrie (2012), The age and rate of displacement along the Main Central Thrust in the western Bhutan Himalaya, *Earth Planet. Sci. Lett.*, *319–320*, 146–158, doi:10.1016/j.epsl.2011.12.005.

Turcotte, D. L., and G. Schubert (2002), *Geodynamics*, 458 pp., Cambridge Univ. Press, Cambridge, U. K.

Wagner, T., J. Lee, B. R. Hacker, and G. Seward (2010), Kinematics and vorticity in Kangmar Dome, southern Tibet: Testing mid-crustal channel-flow models for the Himalaya, *Tectonics*, *29*, TC6011, doi:10.1029/2010TC002746.

Warren, C., D. Grujic, D. A. Kellett, J. M. Cottle, R. A. Jamieson, and K. Ghalley (2011), Probing the depths of the India-Asia collision: U-Th-Pb monazite chronology of granulites from NW Bhutan, *Tectonics*, *30*, TC2004, doi:10.1029/2010TC002738.

Webb, A. A. G., A. Yin, T. M. Harrison, J. Célérier, and W. P. Burgess (2007), The leading edge of the Greater Himalayan Crystalline complex revealed in the NW Indian Himalaya: Implications for the evolution of the Himalayan orogen, *Geology*, *35*, 955–958, doi:10.1130/G23931A.1.

Webb, A. A. G., A. K. Schmitt, D. He, and E. L. Weigand (2011), Structural and geochronological evidence for the leading edge of the Greater Himalayan Crystalline complex in the central Nepal Himalaya, *Earth Planet. Sci. Lett.*, *304*, 483–495, doi:10.1016/j.epsl.2011.02.024.

Wells, M. L., and T. D. Hoisch (2008), The role of mantle delamination in widespread Late Cretaceous extension and magmatism in the Cordilleran orogen, western United States, *Geol. Soc. Am. Bull.*, *120*, 515–530, doi:10.1130/B26006.1.

Wernicke, B. (2009), The detachment era (1977–1982) and its role in revolutionizing continental tectonics, *Geol. Soc. Spec. Publ.*, *321*, 1–8, doi:10.1144/SP321.1.

Wernicke, B., and B. C. Burchfiel (1982), Modes of extensional tectonics, *J. Struct. Geol.*, *4*, 105–115, doi:10.1016/0191-8141(82)90021-9.

Wernicke, B., G. J. Axen, and J. K. Snow (1988), Basin and Range extensional tectonics at the latitude of Las Vegas, Nevada, *Geol. Soc. Am. Bull.*, *100*, 1738–1757, doi:10.1130/0016-7606(1988)100<1738:BARETA>2.3.CO;2.

Wernicke, B., J. L. Davis, N. A. Niemi, P. Luffi, and S. Bisnath (2008), Active megadetachment beneath the western United States, *J. Geophys. Res.*, *113*, B11409, doi:10.1029/2007JB005375.

Whitney, D. L., and B. W. Evans (2010), Abbreviations for names of rock-forming minerals, *Am. Mineral.*, *95*, 185–187, doi:10.2138/am.2010.3371.

Wiesmayr, G., and B. Grasemann (2002), Eohimalayan fold and thrust belt: Implications for the geodynamic evolution of the NW-Himalaya (India), *Tectonics*, *21*(6), 1058, doi:10.1029/2002TC001363.

Wu, C., K. D. Nelson, G. Wortman, S. D. Samson, Y. Yue, J. Li, W. S. F. Kidd, and M. A. Edwards (1998), Yadong cross structure and South Tibetan Detachment in the east central Himalaya (89°–90°E), *Tectonics*, *17*, 28–45, doi:10.1029/97TC03386.

Xypolias, P., and S. Kokkalas (2006), Heterogeneous ductile deformation along a mid-crustal extruding shear zone: An example from the External Hellenides (Greece), in *Channel Flow, Ductile Extrusion and Exhumation in Continental Collision zones*, edited by R. D. Law, M. P. Searle, and L. Godin, *Geol. Soc. Spec. Publ.*, *268*, 497–516.

Yin, A. (2006), Cenozoic tectonic evolution of the Himalayan orogen as constrained by along-strike variation of structural geometry, exhumation history, and foreland sedimentation, *Earth Sci. Rev.*, *76*, 1–131, doi:10.1016/j.earscirev.2005.05.004.

D. Grujic, Department of Earth Sciences, Dalhousie University, Halifax, NS B3H 4J1, Canada.

D. A. Kellett, Geological Survey of Canada, 601 Booth St., Ottawa, ON K1A 0E8, Canada. (dawn.kellett@nrcan.gc.ca)